Ecological Indicators 131 (2021) 108147

Contents lists available at ScienceDirect

Ecological Indicators

journal homepage: www.elsevier.com/locate/ecolind

Original Articles

Monitoring agroecosystem productivity and phenology at a national scale: A metric assessment framework

Dawn M. Browning [a,*], Eric S. Russell [b], Guillermo E. Ponce-Campos [c], Nicole Kaplan [d], Andrew D. Richardson [e,f], Bijan Seyednasrollah [e,f], Sheri Spiegal [a], Nicanor Saliendra [g], Joseph G. Alfieri [h], John Baker [i], Carl Bernacchi [j], Brandon T. Bestelmeyer [a], David Bosch [k], Elizabeth H. Boughton [l], Raoul K. Boughton [l], Pat Clark [m], Gerald Flerchinger [m], Nuria Gomez-Casanovas [n], Sarah Goslee [o], Nick M. Haddad [p], David Hoover [d], Abdullah Jaradat [s], Marguerite Mauritz [q,r], Gregory W. McCarty [h], Gretchen R. Miller [t], John Sadler [u], Amartya Saha [l], Russell L. Scott [v], Andrew Suyker [w], Craig Tweedie [t], Jeffrey D. Wood [u], Xukai Zhang [l], Shawn D. Taylor [a]

[a] U.S. Department of Agriculture – Agricultural Research Service, Las Cruces, NM 88003, United States
[b] Dept. Civil and Environmental Engineering, Washington State University, Pullman, WA 99164, United States
[c] School of Natural Resources and Environment, University of Arizona, Tucson, AZ 85721, United States
[d] U.S. Department of Agriculture – Agricultural Research Service, Fort Collins, CO 80526, United States
[e] Center for Ecosystem Science and Society, Northern Arizona University, Flagstaff, AZ 86011, United States
[f] School of Informatics, Computing and Cyber Systems, Northern Arizona University, Flagstaff, AZ 86011, United States
[g] U.S. Department of Agriculture – Agricultural Research Service, Mandan, ND 58554, United States
[h] U.S. Department of Agriculture – Agricultural Research Service, Beltsville, MD 20705, United States
[i] U.S. Department of Agriculture – Agricultural Research Service, St. Paul, MN 55108, United States
[j] Global Change and Photosynthesis Research, USDA-ARS, Urbana, IL 61801, United States
[k] U.S. Department of Agriculture – Agricultural Research Service, Tifton, GA, 31794, United States
[l] Archbold Biological Station's Buck Island Ranch, Lake Placid, FL 33852, United States
[m] U.S. Department of Agriculture – Agricultural Research Service, Boise, ID 83702, United States
[n] Institute for Sustainability, Energy, and Environment, University of Illinois at Urbana-Champaign, Urbana, IL 61820, United States
[o] U.S. Department of Agriculture – Agricultural Research Service, University Park, PA 16802, United States
[p] Kellogg Biological Station and Department of Integrative Biology, Michigan State University, Hickory Corners, MI 49060, United States
[q] Environmental Science and Engineering, University of Texas at El Paso, TX 79902, United States
[r] Biological Sciences, University of Texas at El Paso, TX 79902, United States
[s] U.S. Department of Agriculture – Agricultural Research Service, Morris, MN 56267, United States
[t] Department of Civil and Environmental Engineering, Texas A&M University, College Station, TX 77843-3136, United States
[u] School of Natural Resources, University of Missouri, Columbia, MO 65211, United States
[v] U.S. Department of Agriculture – Agricultural Research Service, Tucson, AZ 85719, United States
[w] University of Nebraska, Lincoln, NE 68588, United States

ARTICLE INFO

Keywords:
Agricultural management
Eddy covariance
GPP
Growing season length
Indicators
Long-Term Agroecosystem Research (LTAR) network
Landsat

ABSTRACT

Effective measurement of seasonal variations in the timing and amount of production is critical to managing spatially heterogeneous agroecosystems in a changing climate. Although numerous technologies for such measurements are available, their relationships to one another at a continental extent are unknown. Using data collected from across the Long-Term Agroecosystem Research (LTAR) network and other networks, we investigated correlations among key metrics representing primary production, phenology, and carbon fluxes in croplands, grazing lands, and crop-grazing integrated systems across the continental U.S. Metrics we examined included gross primary productivity (GPP) estimated from eddy covariance (EC) towers and modelled from the Landsat satellite, Landsat NDVI, and vegetation greenness (Green Chromatic Coordinate, G_{CC}) from tower-mounted PhenoCams for 2017 and 2018. Overall, our analysis compared production dynamics estimated from

* Corresponding author.
E-mail address: dawn.browning@usda.gov (D.M. Browning).

https://doi.org/10.1016/j.ecolind.2021.108147
Received 30 June 2021; Received in revised form 18 August 2021; Accepted 23 August 2021
Available online 27 August 2021

PhenoCam
Sustainable agriculture

three independent ground and remote platforms using data for 34 agricultural sites constituting 51 site-years of co-located time series.

Pairwise sensor comparisons across all four metrics revealed stronger correlation and lower root mean square error (RMSE) between end of season (EOS) dates (Pearson R ranged from 0.6 to 0.7 and RMSE from 32.5 to 67.8) than start of season (SOS) dates (0.46 to 0.69 and 40.4 to 66.2). Overall, moderate to high correlations between SOS and EOS metrics complemented one another except at some lower productivity grazing land sites where estimating SOS can be challenging. Growing season length estimates derived from 16-day satellite GPP (179.1 days) were significantly longer than those from PhenoCam G_{CC} (70.4 days, $p_{adj} < 0.0001$) and EC GPP (79.6 days, $p_{adj} < 0.0001$). Landscape heterogeneity did not explain differences in SOS and EOS estimates. Annual integrated estimates of productivity from EC GPP and PhenoCam G_{CC} diverged from those estimated by Landsat GPP and NDVI at sites where annual production exceeds 1000 $gC/m^{-2}\ yr^{-1}$. Based on our results, we developed a "metric assessment framework" that articulates where and how metrics from satellite, eddy covariance and PhenoCams complement, diverge from, or are redundant with one another. The framework was designed to optimize instrumentation selection for monitoring, modeling, and forecasting ecosystem functioning with the ultimate goal of informing decision-making by land managers, policy-makers, and industry leaders working at multiple scales.

1. Introduction

An accurate understanding of agroecosystem dynamics is critical for the design of management and policy strategies in a changing climate. Climate change can alter growing seasons, water availability, and production potential (Tracy et al., 2018). These changes may vary across agroecosystems spanning a wide range of climates, operation scales, production commodities, management practices, and stakeholder perceptions. Monitoring agroecosystems from pasture or field-level to landscape and regional scales is thus necessary to inform management and policy decisions. Currently, efforts to monitor agroecosystems at regional to global scales rely largely on time series data collected from satellite remote sensing (Weiss et al., 2020). Day-to-day management decisions at the field level, however, may be best served by ground-based sensors that validate and verify satellite-derived metrics and provide real-time, fine-scale estimates of crop or forage status (Browning et al., 2015, Fritz et al., 2019). We have little understanding of the varying relationships among sensor platforms in agroecosystems at a national scale, which vary strongly in the amount and timing of production, intensity of management, and degree of spatial heterogeneity.

Here we take advantage of data collected across the Long-Term Agroecosystem Research (LTAR) network to investigate correlations among several key ecosystem metrics across the continental U.S., including the consistency of metrics across sensors. We focused on measuring phenology - defined as the timing of recurring events such as germination and flowering, green-up, or senescence - as it is a key multi-scale attribute in agroecosystems that is sensitive to management and climate change. Phenology metrics, offer an effective means to assess the utility of instruments used to monitor land surface dynamics in diverse agricultural production systems. For instance, the phenological state of different crops dictates the timing of pollination and pest and fertilizer treatments, while livestock production can be optimized by matching animal densities and distributions to seasonal dynamics in forage production (Browning et al., 2017, Seo et al., 2019). However, such fine scale phenological information is not often available to land managers, and is further complicated by changing growing seasons. Shifts in growing seasons in response to climate change have been reported across many ecosystems worldwide (Kukal and Irmak, 2018), with regional differences in the timing and magnitude of change (Buitenwerf et al., 2015, Garonna et al., 2016). Increased global greenness has been attributed to an elongated growing season resulting from changing crop phenology (Gao et al., 2019). Phenology metrics, such as start and end of the growing season and growing season length, can be used to estimate the timing and amount of primary production along with its seasonal and interannual variation. Thus, understanding patterns such as the start, end, length, and shape of the growing season defined via multiple metrics is key to integrating data across diverse sites and sensors to better understand past trends and forecast future ones (Toomey et al., 2015,Wu et al., 2017, Richardson et al., 2018b).

The USDA Agricultural Research Service LTAR network, singly and in partnership with other networks, provides consistent measurements across locations that span production system types, climatic and productivity gradients (Baffaut et al., 2020). Management activities at these locations can result in abrupt changes in biomass, such as end of season harvest, or gradual changes, such as the use of fertilizers that progressively enhance biomass over the growing season. Changes in biomass due to management may or may not be discernible depending on the limits of detection. For example, heavy grazing due to high livestock density on a pasture can be readily detected due to rapid decreases in aboveground biomass (Fan et al., 2011) whereas low density livestock grazing may be undetectable or even increase aboveground biomass through compensatory growth and/or manure fertilization (Belsky, 1986, Milchunas and Lauenroth, 1993, Frank and McNaughton, 1993, Briske et al., 2008). High spatial and temporal heterogeneity is inherent to agricultural landscapes (Hank et al., 2015), and requires the use of field-scale sensors such as eddy covariance towers and PhenoCams to detect important variations in phenology. To improve and extend monitoring of agroecosystems to broader spatial extents, it is critical to integrate data from both ground-based and satellite sensors. Thus, it is necessary to compare the strengths and limitations of productivity metrics across platforms and identify instances where satellite and ground-based sensors are redundant, diverge from, or complement one another. A deeper understanding of these relationships is made possible by sensor networks that share consistent data collection and data management protocols that produce interoperable data streams.

Several locations in the LTAR network are associated with, or share data with other research networks, such as the PhenoCam Network (Richardson et al., 2018a), National Ecological Observatory Network (NEON; Keller et al., 2008), AmeriFlux (Novick et al., 2018), and Long-Term Ecological Research Network (LTER; Knapp et al., 2012). Coordinated, co-located collection of high resolution datasets, via partnership among research networks, provides wider coverage of PhenoCam imagery, eddy covariance-derived fluxes, and meteorological measurements. Ground-based sensor data also complement the diversity of remote sensing applications in agriculture (Weiss et al., 2020, Reinermann et al., 2020), which currently make it difficult to track the wide array of local management practices using a common ontology at a nationwide scale.

For some applications, remotely-sensed data may be sufficient (e.g., Smith et al., 2019), but may not have sufficient spatiotemporal resolution needed to monitor diverse agricultural landscapes and meet land management needs for rapid decisions at fine scales. Dependence on data products derived from satellite remote sensing in places where these products do not accurately represent the production dynamics (due to large pixel size, obstruction by cloud cover, long return cycles and lack of ground validation) can foster uncertainty for land managers

(e.g., Butterfield and Malmström, 2009). Cases where satellite-derived and ground-based metrics are commensurate and well-correlated create opportunities to scale up interpretations of local information more broadly. In cases where satellite-derived and ground-based metrics are divergent, near-surface digital cameras, or PhenoCams, offer daily images to link ground-based and remotely-sensed metrics (e.g., Browning et al., 2017, Norris and Walker, 2020).

Several prior studies compared near-surface and satellite sensors at regional and continental scales (Balzarolo et al, 2016; Klosterman et al., 2014, Toomey et al., 2015, Wu et al., 2017). There are cases of strong correlation between growing season metrics (SOS and EOS) from PhenoCam and eddy covariance in plant communities with distinct phenological profiles such as deciduous broadleaf forests (Toomey et al., 2015). In addition, there are those of low correlation between estimated SOS and EOS dates from MODIS vegetation index values and eddy covariance that can be improved depending on plant functional type and the fitting algorithm used (Wu et al., 2017). Satellite and near-surface sensors (i.e., PhenoCam and eddy covariance) generally agree as long as the temporal and/or spatial resolutions of satellite data are not too coarse, and the landscape is homogeneous (Yan et al., 2019, Richardson et al., 2018b). Browning et al. (2017) evaluated agreement between greenness metrics from satellite and PhenoCam in a desert grassland system and found good agreement when the focal species in the PhenoCam analysis was a conspicuous shrub, but not so when the focal species was a less abundant perennial grass. Even in arid systems with mixed vegetation, PhenoCams worked well when the focal species represented the system.

In this study, we hypothesized that growing season metrics from satellite and near-surface sensors would be correlated and that the strength of the relationships vary depending on the scale of observation and spatial heterogeneity. Given a homogenous landscape, indices of vegetation greenness and primary productivity derived from satellite and near-surface optical sensors are expected to yield similar estimates for phenological transition dates despite differences in spatial resolution. As landscape heterogeneity increases due to different land cover types, vegetation structure, and/or agricultural practices, the correspondence of phenology and productivity estimates from different tools or sensors may decrease (Richardson et al., 2018b). For example, the spatial scale of a tower-mounted digital camera (i.e., PhenoCam) can vary with configuration and typically captures a portion of a single field, while modeled estimates of gross primary production from satellite (GPP; Robinson et al., 2018) are aggregated over 0.8 ha circa multiple 30-m pixels (or considerably coarser for MODIS) and could incorporate several crop types and possibly non-agricultural areas. Eddy covariance towers are typically situated to sample a specific crop or ecosystem, but their footprint often exceeds a hectare in size and the CO_2 flux measurement footprint changes dynamically in response to shifts in wind speed and direction. Notably, while satellite estimates and flux tower measurements can only measure land-cover trends in aggregate (Browning et al., 2017; Yan et al., 2019), PhenoCams can identify phenological profiles of specific elements in the camera field of view (e.g., plant functional group or cropping system).

2. Objectives and questions

We aim to use our analysis as a foundation for optimizing the choice of instruments for agroecosystem monitoring by: 1) evaluating differences in phenology metrics derived from three different sensor platforms in different U.S. agroecosystems and 2) using these comparisons to develop a novel "metric assessment framework" to help researchers and managers identify instances where satellite and ground-based sensors are redundant to, diverge from, or complement one another.

Our specific research questions were:

Among sensors (eddy covariance, PhenoCam, and satellite), what is the correlation between phenology metrics [start of season (SOS), end of season (EOS), season length, and related daily and annual estimates of timing and amount of production]?

Do differences in temporal and spatial scale of sensor metrics account for variability in SOS and EOS?

Does the degree of site heterogeneity (e.g., surrounding land cover classes or cropping systems) correlate with variation in pairwise comparisons of metrics?

3. Data and methods

3.1. Network sites

The USDA Agricultural Research Service LTAR is a network of 18 locations collaborating to evaluate strategies for the sustainable intensification of agriculture in croplands, rangelands, and integrated crop-livestock systems nationwide. Integrated crop-livestock systems use both; in some cases livestock graze the crops directly and in others they do not. LTAR locations spanning cropland, grazing, and integrated crop-livestock production systems represent a diversity of land production potentials, climates, management approaches, and agricultural products (Spiegal et al., 2018). The network represents roughly 49% of the cereal production, 30% of the forage production, and 32% of the livestock production in the United States (Kleinman et al., 2018).

We obtained data from 15 of the LTAR locations where production and phenology metrics were available to meet the criterion of having co-located PhenoCam and eddy covariance data for years 2017 and 2018. For clarity, we refer to study sites as 'locations' and use the word 'site' to refer to instrumented towers; in 12 cases, locations have more than one contributing site. We also included two managed locations in NEON (Konza Prairie Agroecosystem, Jornada LTER) and two in the LTER network (Kellogg Biological Station, Sevilleta). Jornada Basin is a location in all three networks (Supplemental Fig. 1). All sites used in the analysis conduct rainfed agriculture except PRHPA *mead1* and *mead2* sites (center pivot irrigation), and the ABS-UF pasture site (*archboldpnot*) which receives occasional pump irrigation during the dry season in Florida (Nov-Apr; Baffaut et al., 2020). Site names are found in Table 1.

Long-term (1981–2010) mean annual temperature and rainfall for sites in this study range from 5.6 °C (at Northern Plains and Great Basin LTAR locations) to 22.7°C (ABS-UF LTAR location) and from 200 mm (Sevilleta LTER location) to 1084 mm (ABS-UF LTAR location), respectively (Supplemental Table 1). There were regional differences in mean annual temperature and annual precipitation in 2017 and 2018 (Fig. 1). In general, the water-limited sites in the southwest U.S were warmer than average in both study years. In 2018, most of the sites, particularly those in the eastern US, were substantially wetter than average. Precipitation in 2018 for the Great Basin LTAR sites was approximately 80% of the long-term average.

3.2. Sensor data

3.2.1. Canopy greenness data from PhenoCams

PhenoCam data for the study sites were obtained from the PhenoCam Dataset V2.0 (Seyednasrollah et al., 2019a; Seyednasrollah et al., 2019b; Milliman et al., 2019). For the PhenoCam sites used in this study, digital images were collected at 30-minute intervals continuously from 4 am to 10 pm. Canopy greenness time series data were obtained from these images by delineating appropriate regions of interest (ROIs), defined by site investigators, and calculating the green chromatic coordinate (G_{CC}) for each ROI as:

$G_{CC} = G_{DN}/(R_{DN} + G_{DN} + B_{DN})$ where R_{DN}, G_{DN} and B_{DN} are the average red, green and blue digital numbers inside the ROIs, respectively. After extracting G_{CC} values, time series were obtained from the 90th percentile of canopy greenness at 3-day intervals for use in estimating phenological transition dates. In comparison to the 1-day time series data, the 3-day time series data are more robust with regard to random noise and hence they are used in this analysis. Details about the

Table 1
Details for 34 PhenoCam and eddy covariance towers (constituting 51 site-years) used in this study along with details of the eddy covariance data sourcing and processing.

Location	Location (State)	EC Tower	Phenocam Name	Production system	EC Processing Reference	EC Data Source	EC Site
ABS-UF	FL	archboldpnot	archboldpnot	grazing	Gomez-Casanovas et al., 2020	LTAR	US-IL1
ABS-UF	FL	ufona	ufona	grazing	Gomez-Casanovas et al., 2020	LTAR	US-ONA
CAF	WA	boydnorth	cafboydnorthltar01	cropland	Russell et al., 2019	Ameriflux	US-CF1
CAF	WA	cookeast	cafcookeastltar01	cropland	Russell et al., 2019	Ameriflux	US-CF2
CAF	WA	cookwest	cafcookwestltar01	cropland	Russell et al., 2019	Ameriflux	US-CF3
CMRB	MO	asp	goodwater	cropland	Wood et al., 2019	LTAR	US-Mo1
CPER	CO	agm	cperagm	grazing	NA	LTAR	US-CX2
CPER	CO	tgm	cpertgm	grazing	NA	LTAR	US-CX1
GACP	GA	arsgacp1	arsgacp1	integrated	Russell et al., 2019	LTAR	NA
GACP	GA	arsgacp2	arsgacp2	integrated	Russell et al., 2019	LTAR	NA
GB		arsgreatbasinltar098	arsgreatbasinltar098	grazing	Flerchinger et al., 2020	LTAR	US-Rws
JORN	NM	jerbajada	jerbajada	grazing	NA	LTAR	US-Jo1
JORN	NM	neon	NEON.D14.JORN.DP1.00033	grazing	Metzger et al., 2019	NEON	NEON.D14.JORN.DP4.00200.001
KBS	MI	T3	kelloggcorn	cropland	Abraha et al., 2015	LTER	US-KM1
KONA	KS	KONA	NEON.D06.KONA.DP1.00033	cropland	Metzger et al., 2019	NEON	NEON.D06.KONA.DP4.00200.001
LCB	MA	op3	arsope3ltar	integrated	NA	LTAR	US-OPE
NP	ND	h5	mandanh5	cropland	Saliendra et al., 2018	LTAR	US-NP1
NP	ND	i2	mandani2	cropland	Saliendra et al., 2018	LTAR	US-NP2
PRHPA	NE	mead1	mead1	cropland	Suyker et al., 2005	LTAR	US-Ne1
PRHPA	NE	mead2	mead2	cropland	Suyker et al., 2005	LTAR	US-Ne2
PRHPA	NE	mead3	mead3	cropland	Suyker et al., 2005	LTAR	US-Ne3
PRHPA	NE	meadpasture	meadpasture	grazing	Suyker et al., 2005	LTAR	NA
SEG	NM	grasslands	sevilletagrass	grazing	Anderson-Teixeira et al., 2011	Ameriflux	US-Seg
SEG	NM	shrublands	sevilletashrub	grazing	Anderson-Teixeira et al., 2011	Ameriflux	US-Ses
TG	TX	tworfpr	tworfpr	integrated	NA	LTAR	US-Tx2
UCB	PA	hawbeckereddy	hawbeckereddy	integrated	Skinner, 2008	LTAR	US-HWB
UMRB	MN	morrisnorth	arsmorris1	cropland	Saliendra et al., 2018	LTAR	NA
UMRB	MN	morrissouth	arsmorris2	cropland	Saliendra et al., 2018	LTAR	NA
UMRB	MN	rosemountcons	rosemountcons	cropland	Griffis et al., 2005	Ameriflux	US-Ro4
UMRB	MN	rosemountconv	rosemountconv	cropland	Griffis et al., 2005	Ameriflux	US-Ro5
UMRB	MN	rosemountnprs	rosemountnprs	cropland	Griffis et al., 2005	Ameriflux	US-Ro6
WGEW	AZ	Kendall Grassland	kendall	grazing	Scott et al., 2015	Ameriflux	US-Wkg
WGEW	AZ	Lucky Hills Shrubland	luckyhills	grazing	Scott et al., 2015	Ameriflux	US-Whs
NEON-Wood	ND	USxWD	NEON.D09.WOOD.DP1.00033	grazing	Metzger et al., 2019	NEON	NEON.D09.WOOD.DP4.00200.001

PhenoCam dataset and image processing are discussed by Seyednasrollah et al. (2019b), Seyednasrollah et al. (2019c).

3.2.2. Carbon flux data from eddy covariance towers

The eddy covariance data were obtained from three different sources including: the NEON data portal (2 sites), AmeriFlux (4 sites), and directly from the LTAR sites (14 sites). The number of flux towers per location ranged from one at Central Mississippi River Basin LTAR location to four at Platte River High Plains Aquifer LTAR location (see Table 1, Supplemental Fig. 1). Briefly, three-dimensional sonic anemometers and an infrared gas analyzer were mounted above plant canopies to measure the three wind velocity vector components, sonic temperature, and concentrations of water vapor and carbon dioxide at 10 or 20 Hz. These values were processed to 30-minute fluxes of carbon dioxide and water vapor at the individual sites using standardized equations (e.g., Burba, 2013; Aubinet et al., 2012). See Table 1 for more details on the processing and source of the flux data for each site.

While the software to process the eddy covariance data differed between sites, the same post-processing algorithms were used. A custom Python V3 processing script was used to complete the quality assurance and formatting. For the flux data, this step checked that values were within a physically realistic range de-spiking. Data were de-spiked using a 5-day moving window, to remove flux values that deviated by more than three standard deviations of the 5-day mean (Vickers & Mahrt, 1997). Meteorology data were bounds checked and units converted as needed. Relative humidity (RH) values were deleted if RH $< 0\%$ or if RH $> 102\%$. If not provided, saturation vapor pressure was calculated via Buck (1981) for the calculation of vapor pressure deficit. Any specific quality assurance/quality control needs were accomplished on a site-to-site basis as part of the initial compilation and processing of the data.

The flux data were gap-filled using the nighttime respiration method in the stand-alone R version of REddyProc with the net CO_2 flux partitioned into gross primary production (GPP) and ecosystem respiration (Reco) (Reichstein et al., 2005, Wutzler et al., 2018). After gap-filling, the 30-minute data were converted to daily sums and averages for the different flux and meteorology values were computed. GPP was converted to grams of carbon per day (g C m^{-2} day^{-1}) and summed over daily, weekly, and yearly timescales.

3.2.3. Production data from satellite

We included a satellite-derived estimate of Gross Primary Production (GPP) in addition to the commonly-used unitless Normalized Difference Vegetation Index (NDVI) because modeled GPP values provide a straightforward comparison with GPP estimated by eddy covariance. We used the Landsat GPP product by Robinson et al. (2018), which provides GPP values at a 30-m spatial resolution on a 16-day time-step. This product is based on the MOD17 algorithm (MODerate Resolution Imaging Spectroradiometer) (Running et al., 2004) whose coarse

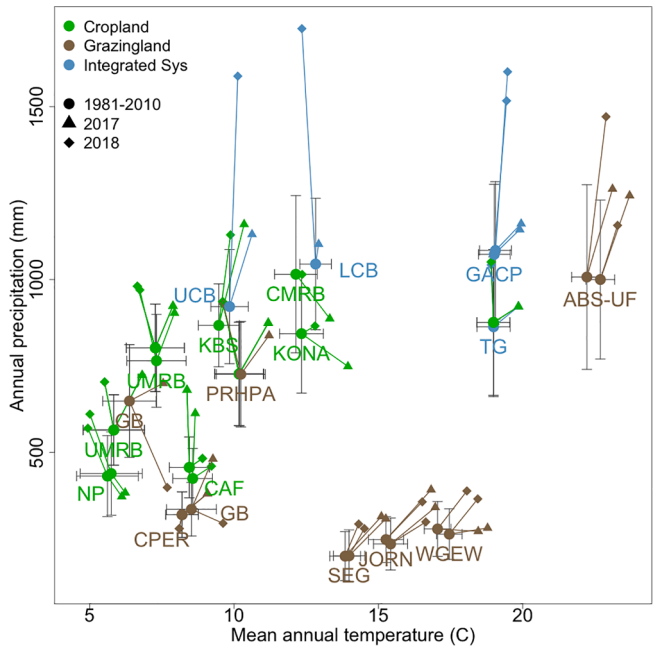

Fig. 1. Thirty year (1981–2010) mean and standard deviation of mean annual temperature and total annual precipitation calculated from the 4-km gridded daily PRISM data for the LTAR PhenoCam sites (PRISM Climate Group, 2004). Deviations from long-term precipitation and temperature for 2017 and 2018 are represented by symbols to put study years in context of long-term normals. Production systems are indicated by color and location names identified with text.

resolution (500-m, Ver. 6) is unable to capture the production response at high spatial resolution. One of the original MOD17 algorithms' main features is that it is not constrained by the spatial resolution of the different parameters used, therefore, inputs with finer spatial resolution and the optimization of parameters that better reflect conditions across the contiguous United States (CONUS) are used to characterize GPP and NPP at 30 m pixel resolution. (Robinson et al., 2018). Even though NDVI is one of the main parameters used in the GPP model, we evaluated it because of its widespread use. NDVI values were computed using a smoothing and climatology approach for gap-filling to create continuous 16-day Landsat composites (Robinson et al., 2017, Robinson et al., 2018).

Using Google Earth Engine, we extracted Landsat GPP at each PhenoCam tower location to pair with corresponding PhenoCam and flux tower data. Modeled Landsat GPP values were aggregated to 90x90-m (3x3 30-m pixels) to be commensurate with flux tower footprints (Li et al., 2008) and PhenoCam fields of view that can range depending on sensor configuration (e.g., circa 7300-m^2 area estimated by Browning et al., 2017). The original values of Landsat GPP were transformed from kg C m^{-2} 16-day^{-1} to g C m^{-2} day^{-1} to make pairwise comparisons with the daily PhenoCam and flux tower measurements.

3.3. Estimating season start and end date

For each site in the analysis, there are four time series: 1) PhenoCam G_{CC}, 2) eddy covariance (EC) flux measurement derived GPP, 3) Landsat NDVI, and 4) Landsat-derived GPP. The PhenoCam and EC flux tower measurements are daily while the Landsat GPP and NDVI values are reported every 16 days. For every available year of each time series and for each of the three data streams we estimated the start and end of the growing season based on the rising/falling method described in Seyednasrollah et al. (2019b). The PhenoCam dataset provides a pre-processed transition date product, while the two GPP datasets were processed separately with the same methodology. Each time series was truncated to a calendar year and smoothed with a locally weighted scatterplot smoothing (LOESS) algorithm. The start of season (SOS) estimate was the first day in which the smoothed time series reached 50% of the maximum value of GPP or G_{CC}, and the end of season (EOS) estimate was the last day of each calendar year when the smoothed time series dropped below 50% of the maximum values. Before choosing the 50% threshold, we also tested thresholds of 10% and 25%. A 25% threshold had similar correspondence among the three data streams for all towers (data not shown). The 10% threshold had very low correspondence due to the higher uncertainty signified by the lower initial slope of greenness curves and high daily variability in the three time series, especially in dormant periods.

We characterized growing season patterns (i.e., phenological profiles) by amplitude and shape of annual curves. In addition, we tabulated growing season length (GSL) as the difference between EOS and SOS for each year, site and sensor combination.

3.4. Comparing phenology and productivity metrics and landscape heterogeneity

3.4.1. Phenology metrics

To evaluate correlations among SOS and EOS metrics from different sensors, we made six pairwise comparisons of SOS and EOS dates among all sites (i.e., PhenoCam vs EC GPP, PhenoCam vs satellite GPP, EC GPP vs satellite GPP, satellite NDVI vs satellite GPP, satellite NDVI vs EC GPP, and satellite NDVI vs PhenoCam) and calculated the Pearson correlation coefficient for each combination. Not all towers had complete years for all three data sets, thus the sample sizes for each comparison vary slightly. We tested for differences in GSL using a 2-way ANOVA (sensor × production system) and used a post-hoc Tukey test to identify the pairwise differences.

We examined correlations between annual productivity estimated as the total in-season integral for all time series via six pairwise comparisons between sites. The in-season integral was computed as the sum of the smoothed time series within the bounds of SOS and EOS dates. This corresponds to the annual GPP for the EC and satellite time series, and provides a unitless measure of summed G_{CC} that has previously shown to be correlated with GPP (Toomey et al., 2015, Hufkens et al., 2016).

3.4.2. Landscape heterogeneity

We assessed how site heterogeneity affects the mismatch of transition date estimates from different sensors. We used the 30-m Cropland Data Layer (CDL, USDA-NASS, 2021) to calculate, for each tower and year, the Shannon diversity index (H) of all pixels within a 100-m radius (Shannon, 1948, Turner, 1989). We fit six linear models, one for each pairwise sensor comparison, using H as an explanatory variable and the absolute difference in transition dates as the response, with the expectation that transition date mismatch would rise with increasing heterogeneity of surrounding cropland (i.e., a positive slope).

3.5. Aggregating management information

To provide management context for selected agroecosystems, we present the sensor time series at two LTAR network (one cropland and one grazing land) sites in 2017 and 2018. The Upper Mississippi River Basin (UMRB) ARS research location in Stevens County, MN (45.6838°, −95.8005°) has towers deployed in two adjacent fields planted with soybeans in 2017 and wheat or corn in 2018. The UMRB cropland site experienced a range of management activities on two fields across two growing seasons. The first field, Field 1 South, was planted with soybeans in 2017 and with corn in 2018. The second field, Field 2 North, was planted with soybeans in 2017 and wheat in 2018 followed by a cover crop planted in late 2018.

At Central Plains Experimental Range (CPER) in Weld County, CO, (40.8330°, −104.760°) towers are in part of an experiment comparing the effects of traditional rangeland management (TRM; 10 herds in 10

pastures) with collaborative adaptive rangeland management (CARM; a single large herd rotated among 10 pastures) (Wilmer et al., 2018). At CPER, the single large herd was rotated into the 123-ha (CARM) pasture in June of 2017 (244 head of cattle) and late July of 2018 (280 head), with each instance lasting approximately-two weeks. These short-term, high intensity grazing events in the CARM treatment pasture were contrasted with the traditional moderate intensity grazing treatment (TRM) pasture (23 head in 2017 and 26 head in 2018 from early May to late September).

4. Results

4.1. Phenological profiles across LTAR network and platforms

Phenological profiles for croplands had the highest daily GPP with a single peak in productivity that was common across all sensor types (Fig. 2). Grazing sites had lower daily GPP overall (relative to cropland sites) and exhibited high between-site variability for all sensors (Fig. 2B, E, H, K). Productivity profiles for integrated system sites had multiple peaks in productivity across all sensors, with maximum GPP values slightly lower than croplands (Fig. 2C, F, I). Across sensors, GPP from eddy covariance towers demonstrated the highest daily and annual between-site variability while satellite GPP had the lowest. Among production systems, croplands exhibited the least inter-annual variability with integrated systems and grazing sites exhibiting the most variability between 2017 and 2018 growing seasons (Fig. 2A, D, G, H).

Mean growing season length (GSL) was significantly different across production systems ($F = 12.06$, $df = 2$, $p < 0.0001$) and metric type ($F = 36.4$, $df = 3$, $p < 0.0001$). Growing season length estimates derived from 16-day Satellite GPP (179.1 days) were significantly longer than those from PhenoCam GCC (70.4 days, $p_{adj} < 0.0001$) and EC GPP (79.6 days, $p_{adj} < 0.0001$). Comparison of estimates of GSL by metric type revealed mean GSL from satellite GPP and NDVI was longer than estimates from PhenoCam G_{CC} ($p_{adj} < 0.0001$) and EC GPP ($p_{adj} < 0.0001$; see Supp. Table 2). GSL from PhenoCam G_{CC} and EC GPP were not significantly different ($p_{adj} = 0.888$). Mean GSL differed significantly among production systems and pairwise comparisons revealed that mean GSL for cropland sites was significantly shorter compared to grazing sites (Fig. 3, $p_{adj} = 0.0001$) and integrated sites ($p_{adj} < 0.0001$) but did not differ between grazing and integrated sites ($p_{adj} = 0.482$; Supp. Table 2).

4.2. Correlations among phenology metrics

Correlations (Pearson r) and root mean square error (RMSE) values between the estimates for EOS across sensors were higher than estimates for SOS (Fig. 4). Pearson correlation for SOS estimates between sensors ranged from 0.46 to 0.69, while EOS estimates had values from 0.50 to 0.70. RMSE values for SOS estimates ranged from 40.4 to 66.2, while EOS estimates ranged from 32.5 to 67.8. The largest RMSE corresponded to EOS estimates between satellite NDVI and EC GPP (Fig. 4L). Outliers for SOS estimates which drove the low correlations were primarily low productivity grazing sites. Dates for 2018 SOS at two grazing sites were

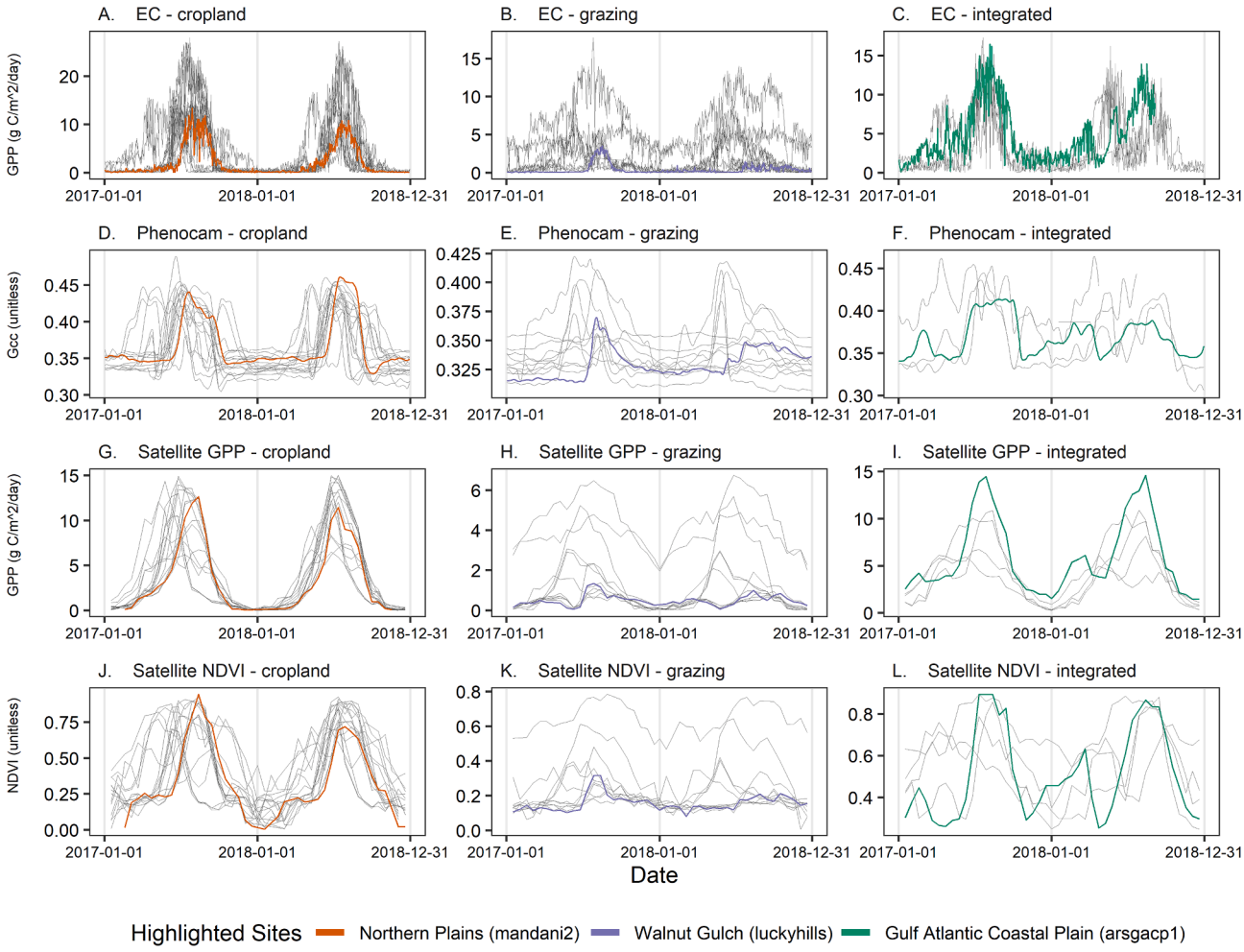

Fig. 2. Summary of daily GPP ($g/m^{-2}/day^{-1}$) from eddy covariance (A-C), G_{CC} vegetation greenness index from PhenoCam (D-F) and GPP (G-I) and NDVI (J-L) from Landsat for the three production system. Gray lines represent individual sites. One site is highlighted per production system with a colored line, with PhenoCam tower names in parentheses in the legend. Y-axis ranges are different for the three production types for clarity.

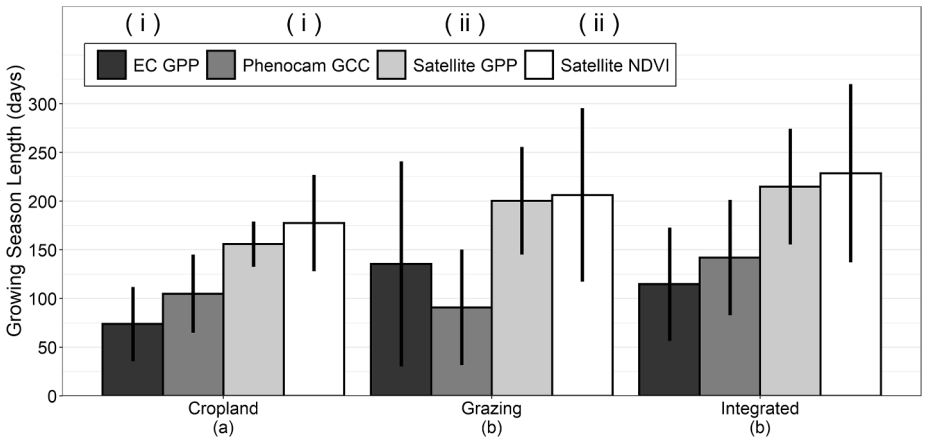

Fig. 3. Mean growing season length (EOS date - SOS date) from eddy covariance GPP, PhenoCam G_{CC}, Landsat GPP and NDVI time series by production system. Error bars represent one SD. Letters in parentheses indicate significant groupings among production systems (along x-axis), and among metric types (along legend) using a 2-way ANOVA.

earlier via EC GPP than via PhenoCam (Fig. 4B) and three were earlier than satellite GPP (Fig. 4C). Specific site references are provided in the Fig. 4 caption.

When clustering along the 1:1 line is considered with the correlation coefficient and RMSE, seasonal start and end dates from PhenoCams and EC had high agreement and low RMSE values (40.4 for SOS, Fig. 4B and 35.0 for EOS, Fig. 4E) even with outlier SOS dates at grazing sites where EC SOS preceded those detected by PhenoCam. The dynamics for EC GPP and PhenoCam G_{CC} are more similar to one another than either is to satellite GPP. Satellite NDVI and GPP were highly correlated as expected given the fact that NDVI is an input to the GPP algorithm. Satellite estimates of SOS were consistently earlier than EC tower estimates. Overall, moderate to high correlations between metrics from different sensors complemented one another with special consideration for lower productivity sites where estimating SOS is more challenging to identify.

4.3. Correlations for production metrics

The annual integral, representing annual productivity for satellite and EC GPP, satellite NDVI, and a unitless metric for PhenoCam G_{CC}, were moderately correlated among all four metrics (Fig. 5). Correlation among the annual integrals was lowest with Phenocam and Satellite GPP measurements (Fig. 5 A). Satellite NDVI had high agreement with the three other sensors (Fig. 5 D, E, F). EC GPP measurements had annual integrals which correlated well with both Satellite NDVI and GPP, and slightly lower for PhenoCam GCC (Fig. 5B, C, E).

Satellite GPP for cropland and integrated sites between 1000 and 1500 gC m^{-2} yr^{-1} exhibited low correspondence and were highly variable for both PhenoCam G_{CC} (Fig. 5A) and EC GPP (Fig. 5C). Thus, the annual estimates of productivity from EC GPP and PhenoCam G_{CC} diverged (i.e., differed strongly) from satellite GPP estimates at sites with annual production above 1000 gC m^{-2} yr^{-1}.

4.4. Effects of landscape heterogeneity on differences in phenology metrics

Landscape heterogeneity had no effect on transition date disagreement for start of season metrics. In all six pairwise comparisons of start of season (SOS), landscape heterogeneity within a 100 m radius had little effect on disagreement between sensors (Fig. 6). We chose the 100 m radius to be conservatively within the tower footprint. Differences in SOS dates for sensor comparisons were highest for the grazing sites identified in Fig. 4C (Fig. 6A-C). There was, however, a significant effect of landscape heterogeneity on differences for EOS estimates between PhenoCam GCC and satellite GPP EOS estimates ($p = 0.017$), satellite NDVI and EC GPP ($p = 0.034$), and satellite NDVI and PhenoCam Gcc ($p = 0.006$), although the explanatory power was low for all three of these cases. (Fig. 7). Negative slopes in the satellite NDVI comparisons (that yielded later EOS estimates) were primarily driven by low productivity grazing sites highlighted as outliers in Fig. 4.

4.5. Metric correspondence in context of management at two sites

For the cropland location (UMRB) growth trajectories (i.e., increasing values) followed planting date and were discernible for all four metrics in both years and fields (Fig. 8A and 8B). Management activities preceding harvest (e.g., tillage, herbicide and fertilizer applications) occurred prior to peak greenness and peak productivity with no noticeable effect on sensor time series. In both fields and growing seasons, harvest had a distinct effect on PhenoCam G_{CC}, where the lowest G_{CC} value occurred at the end of crop senescence, and increased slightly on or around the harvest date (Fig. 8A and B).

The peak of satellite GPP in both cropland fields was offset (earlier) from PhenoCam G_{CC} and EC GPP by several weeks, except for the 2018 corn crop (Fig. 8A). In late 2018 satellite GPP did not show any increase from a growing cover crop, which produced increases in the EC GPP and PhenoCam G_{CC} signals and a prolonged decrease or browndown signal in NDVI.

At the grazing location (CPER) in 2017 there was a noticeable decline in PhenoCam G_{CC} and EC GPP followed by an increase that coincided with the period of high intensity grazing near peak productivity at the CARM pasture (Fig. 8C). In the same year, the 133-ha TRM pasture experienced a similar drop and subsequent increase in PhenoCam G_{CC} and EC GPP, but the timing and magnitude of the drop and rise seemed to differ between the grazing intensity treatments (Fig. 8C and D). In 2018, the high intensity grazing event occurred later in the season, following peak productivity, with less noticeable differences in PhenoCam G_{CC} and EC GPP between the two treatments. Small late season increases in G_{CC} in both pastures occurred in 2017 only.

Certain management activities are readily discerned in the sensor time series (e.g., planting, harvest) and others are not (e.g. herbicide and fertilizer applications in Fig. 8A and B). In addition, satellite GPP did not capture seasonal dynamics of multiple crop growth cycles (Fig. 8B). Detection of grazing effects are specific to time series and grazing practice (Fig. 8 C and D, e.g., large herd for short duration versus smaller herd for longer duration).

5. Discussion

Agroecosystems comprise complex actively-managed landscapes that are vital to sustainably meeting the world's growing demand for

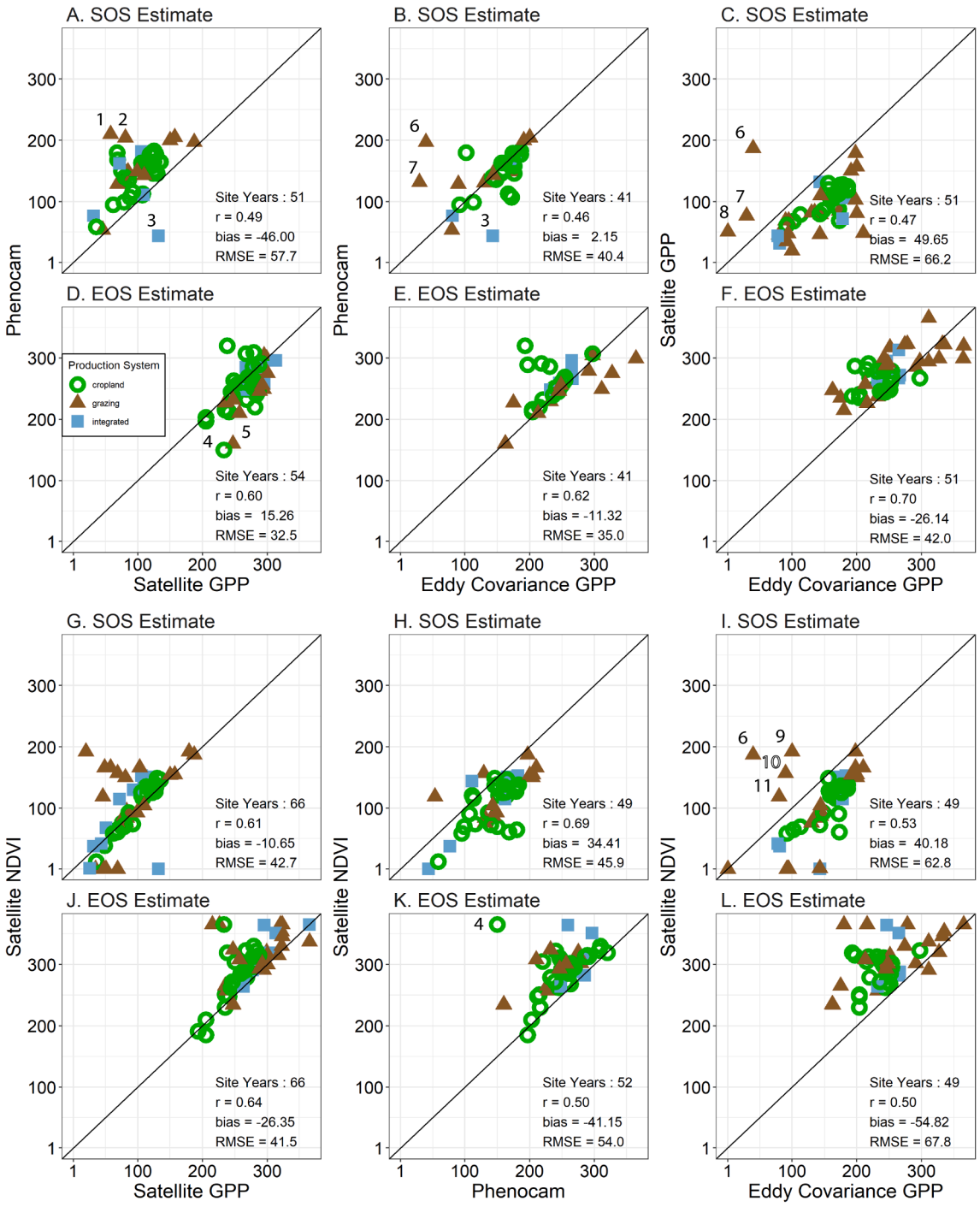

Fig. 4. Six pairwise comparisons of estimated transition dates for start of season (SOS) and end of season (EOS) with Pearson (r) coefficient and RMSE. Comparisons of SOS dates from PhenoCam and satellite GPP (A), PhenoCam and EC GPP (B), and satellite GPP and EC GPP (C) along with EOS dates for the same pairwise comparisons (D, E, and F, respectively). Comparisons for SOS dates from satellite NDVI and satellite GPP (G), satellite NDVI and PhenoCam (H), and satellite NDVI and EC GPP (I) along with EOS dates for the same pairwise comparisons (J, K, L, respectively). The solid line represents the 1:1 line. Point color and shapes respect the three agroecosystem types: cropland, grazing, and integrated sites. The number of site-years analyzed were not the same for all site-sensor combinations. Points considered outliers are identified with numbers representing Site-PhenoCam-year: 1) JER-*jerbajada*-2017, 2) JER-*NEON.D14.JORN.DP1.00033*–2017, 3) GACP-*arsgacp1*-2018, 4) NEON- *NEON.D06.KONA.DP1.00033*–2017, 5) CPER-*cpertgm*-2018, 6) WGEW-*luckyhills*-2018, 7) ABS-UF-*ufona*-2018, 8) LTER-*sevilletashrub*-2018, 9) LTER-*sevilletashrub*-2017, 10) ABS-UF-*archboldpnot*-2018, and 11) ABS-UF-*archboldpnot*-2017.

food. Until recently, agroecosystems were not well-represented in existing research and data networks. Using data from the LTAR and collaborating networks, we offer foundational steps to evaluate relationships among growing season and production metrics.

We hypothesized that high landscape heterogeneity would lead to larger differences in metrics from different sensors. We found no effect of landscape heterogeneity on SOS differences, and a negative effect on EOS differences (Figs. 6 and 7). We selected a conservative radius within 100-m radius of the tower that has been shown to be a reasonable tower footprint (Chu et al., 2021). In the case of EOS estimates higher heterogeneity made sensor estimates more similar. This could be due to low productivity grazing sites having low to no heterogeneity (i.e.,

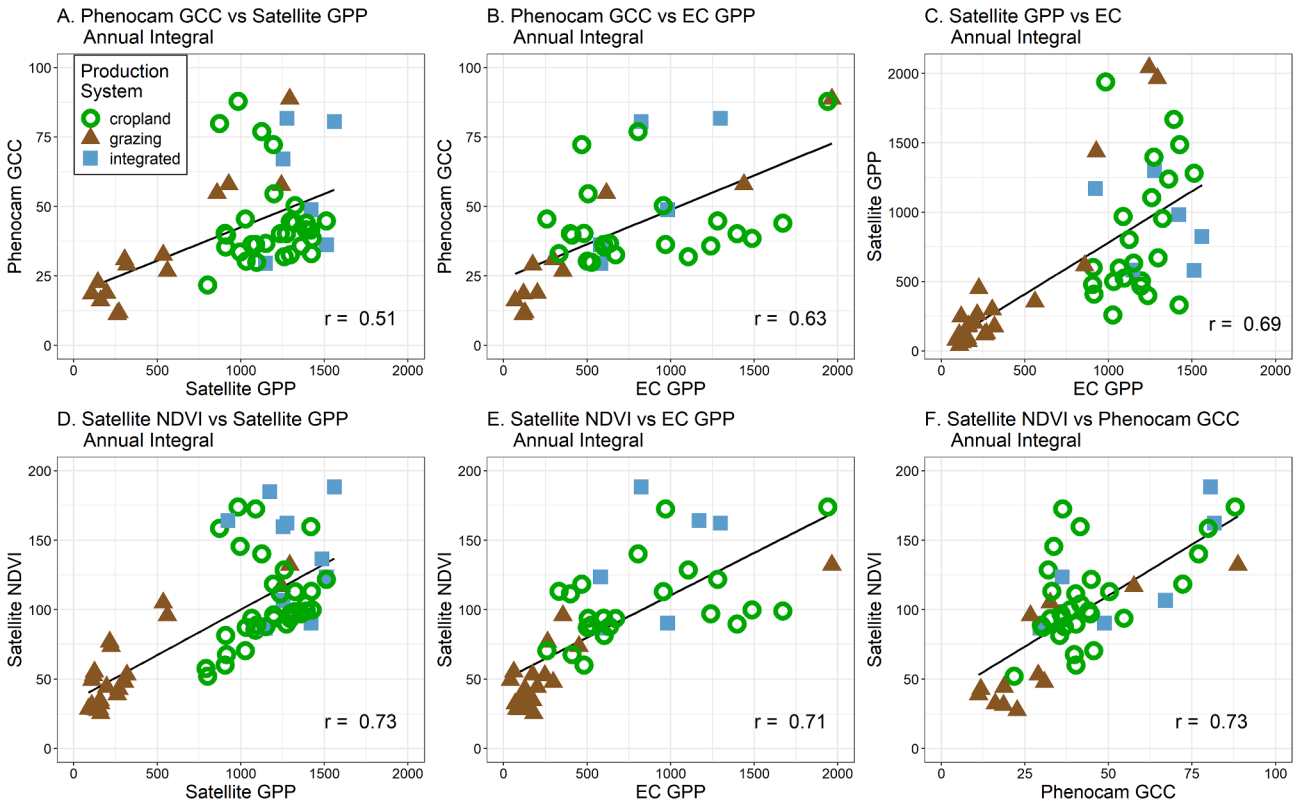

Fig. 5. Relationships between four annual integrated metrics. Season start and end for all data sets were defined using a 50% threshold as in the transition date comparisons. PhenoCam greenness index G_{CC} versus satellite GPP (A), PhenoCam greenness index G_{CC} versus EC GPP (B), and satellite GPP versus EC GPP (C). Second row comparisons represent satellite NDVI versus satellite GPP (D), satellite NDVI versus EC GPP (E), and satellite NDVI versus PhenoCam greenness index G_{CC} (F).

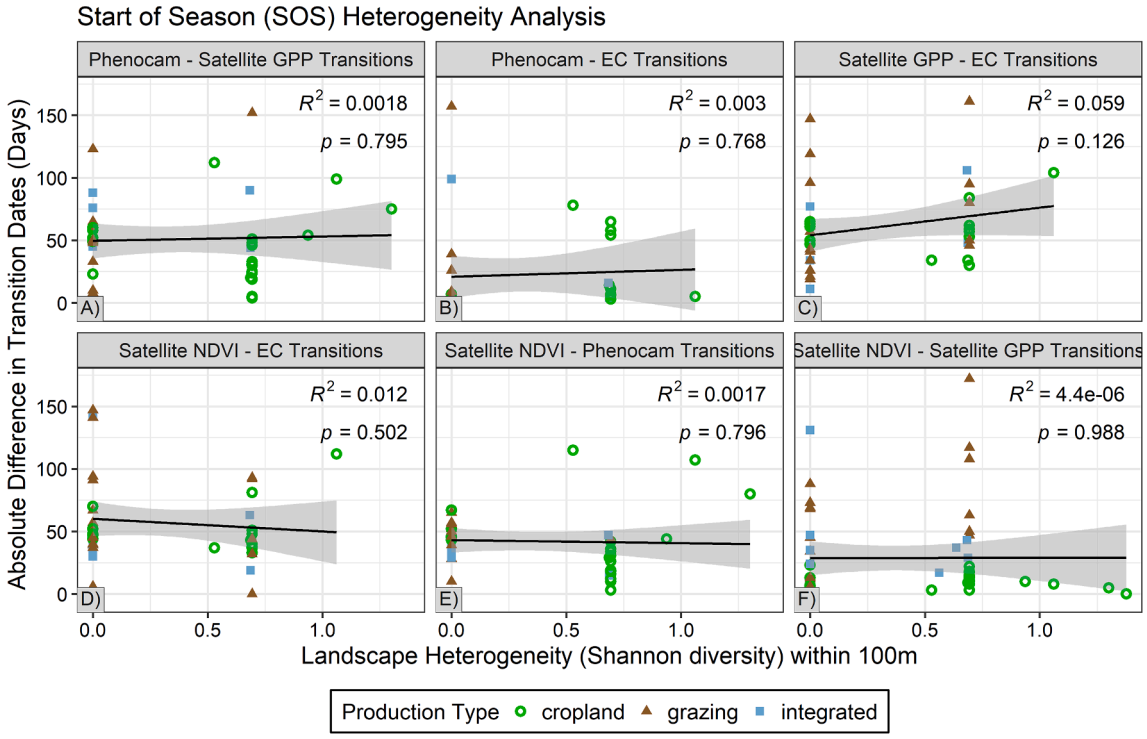

Fig. 6. Absolute difference in SOS transition date estimates (y-axis) between metrics from different sensors explained by landscape heterogeneity using the Shannon diversity index (x-axis). Values near zero indicate similar SOS dates for the two metrics while higher values indicate the first metric corresponds to a later SOS date. Transition dates were defined using a threshold of 50% of the maximum as explained in section 3.3.

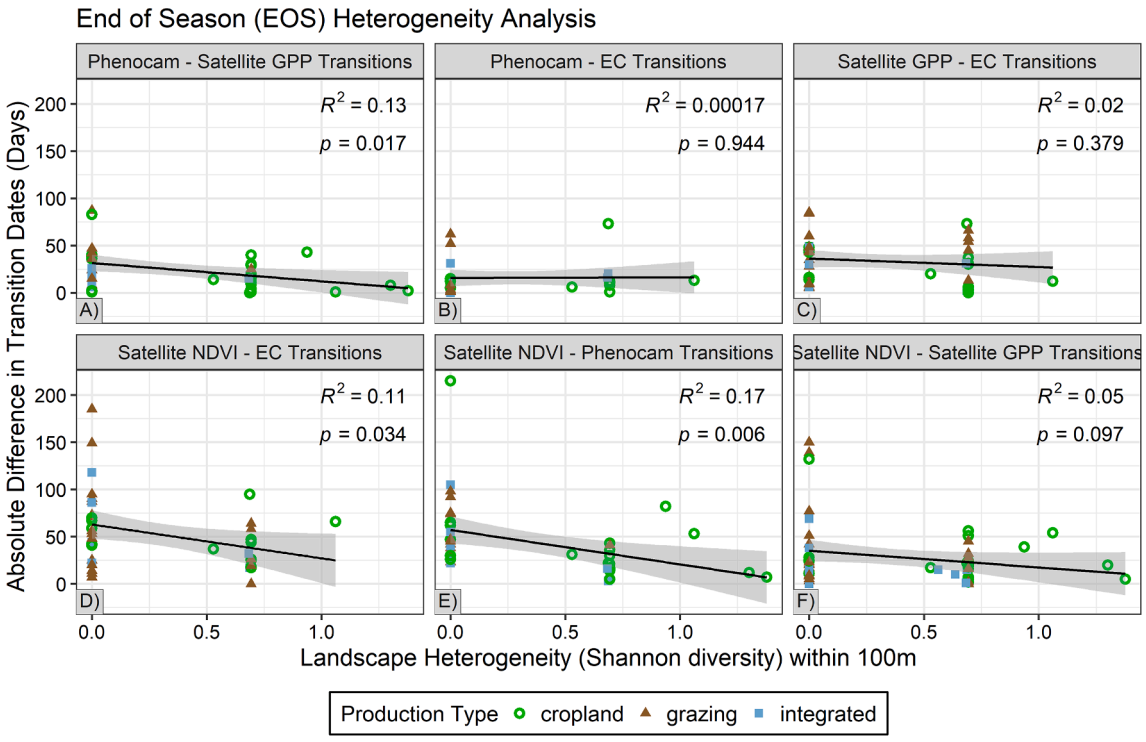

Fig. 7. Absolute difference in EOS transition date estimates (y-axis) between metrics from different sensors explained by landscape heterogeneity using the Shannon diversity index (x-axis). Values near zero indicate similar EOS dates for the two metrics while higher values indicate the first metric corresponds to a later EOS date. Transition dates were defined using a threshold of 50% of the maximum as explained in section 3.3.

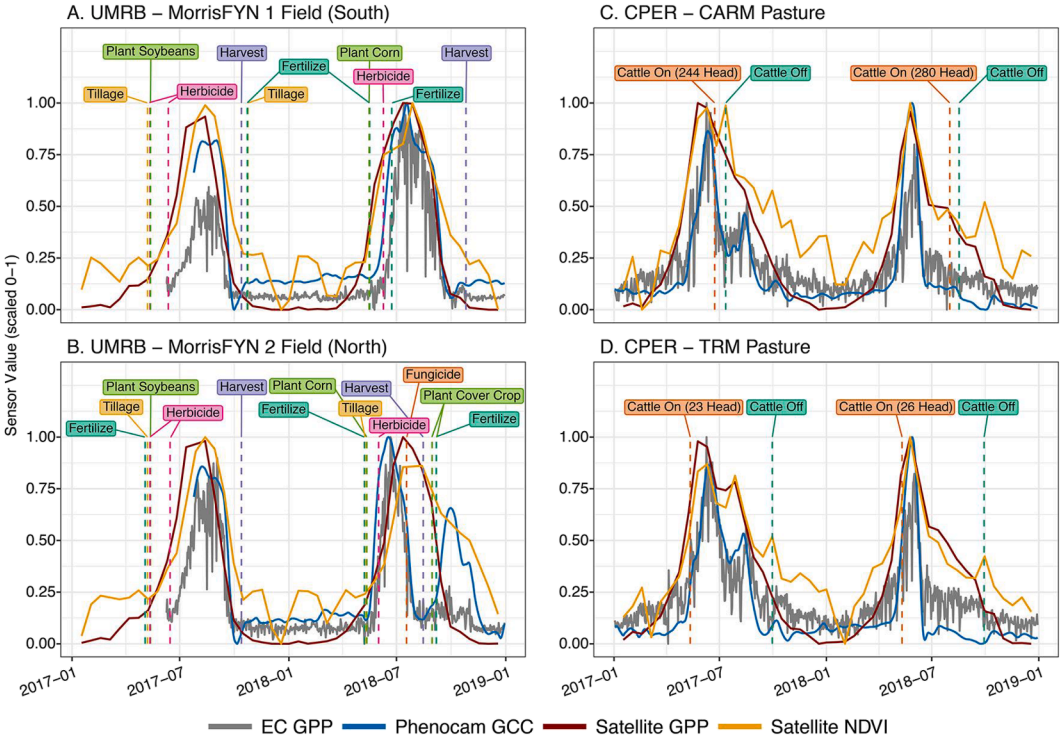

Fig. 8. Time series for GPP from eddy covariance (daily), PhenoCam G_{CC} (daily), GPP and NDVI from Landsat time series (16-day) for four LTAR PhenoCams. Management interventions are denoted by vertical lines. Associated PhenoCam towers are *arsmorris1* (A) and *arsmorris2* (B) for Upper Missouri River Basin locations (UMRB), and *cperagm* (C) and *cpertgm* (D) for Central Plains Experimental Range (CPER) locations. CPER pastures represent the collaborative adaptive rangeland management (CARM, C) and traditional rangeland management (TRM, D). Values are rescaled from 0 to 1 to facilitate comparison across metrics.

consisting of a single land cover pixel type).

Our comparisons of seasonal productivity patterns across 34 U.S. agricultural sites indicate that while metrics produced by different sensors were correlated, correlations between metrics varied across production systems with selected lower productivity grazing lands serving as outliers (Figs. 4 and 5). Below, we consider our findings in the context of complementarity, redundancy, and divergence among sensor metrics.

5.1. Metric assessment framework - complementarity, redundancy, and divergence of metrics

The metric assessment framework is conceptual and can be applied to situations where individuals or groups have access to data from multiple sensors and where decisions regarding optimal sensor use are needed. The framework comprises relationships among metrics including "redundancy", "complementarity", and "divergence" (Fig. 9). This is not an exhaustive list of relationships among metrics and sensors, only the most salient in our experience. We refrain from suggesting specific thresholds for each relationship and instead offer the framework as a flexible approach for optimizing the selection of sensors and metrics for a range of applications.

5.1.1. Redundancy

Redundant metrics are those that are highly correlated and that offer similar interpretation (Fig. 9A). If sensors offer redundant information, users can consider acquisition, installation and maintenance costs for each sensor, personnel costs for processing the data, internet access and risk of vandalism as criteria for selection in the case of resource limitation. Redundant independent metrics can also be helpful for filling data gaps as needed. In this study, we found sensor redundancy between PhenoCam and eddy covariance estimates of EOS and SOS which were well correlated and offered similar transition dates (Fig. 4B). Exceptions most commonly occurred in lower productivity, water-limited grazing systems.

5.1.2. Complementarity

Complementary metrics provide more information together on phenological patterns than each metric does individually. The nature of the relationships is contingent on the management, monitoring, or research goals. If sensors have complementary relationships, decision makers can use the same evaluation criteria described above (in case of redundancy), in addition to considering whether the added information is worth the cost of both instruments (Fig. 9B). In this study, PhenoCam image time series were complementary to both EC and satellite time series by increasing spatial and temporal resolution with ground-level imagery that is captured multiple times daily. The daily near-surface PhenoCam image time series currently offers the capacity to discern phenological profiles for specific plant functional types or crop types (e.g., Browning et al., 2017; Hufkens et al., 2019) and an independent source of land surface phenology with which EC and satellite time series metrics can be verified. Daily time series can be further leveraged to evaluate outlying data points (e.g., Fig. 9B) and devise automated image classification protocols to identify specific plant growth phases. PhenoCams are cost-effective and can be useful for monitoring agricultural production. There is ample opportunity for PhenoCams to complement other sensors by partitioning data into the important phenological periods.

5.1.3. Divergence

Divergent metrics are weakly correlated, provide different signals for the same phenomena that lead to different interpretations and the cause is unknown (Fig. 9C). We highlight three divergent scenarios. The first example of divergence was the poor relationship between annual production values estimated from satellite GPP with either PhenoCam G_{CC} or EC GPP at sites with >1000 gC m^{-2} yr^{-1}. The second case of divergence pertained to SOS dates from NDVI and GPP from satellite for some sites. In these few cases, high NDVI values in early winter led to early SOS estimates not seen in the modelled satellite GPP data product (see grazing land sites in Fig. 4G). Here NDVI can be influenced by gap-filling or low quality pixels, while the derived GPP product constrains these values, resulting in more realistic SOS estimates in these cases.

The third example of divergence was detected in the lower productivity grazing systems in New Mexico and Arizona. This was likely due to flux dynamics in water-limited ecosystems where periods of greenness are decoupled from GPP due to stomatal regulation (Biederman et al., 2017; Yan et al., 2019). Many grazing lands comprise perennial grasses that have extensive shallow (<1 m) root systems. Thus, the onset and end of season measured by uptake differs from patterns of above ground greenness (Delpierre et al., 2016). More research is needed to understand the causes of divergence between sensors. Differences may be related to different scales of detection or measuring different underlying processes. In cases of low correspondence in annual production estimates, one might consider using a different satellite GPP data product (e.

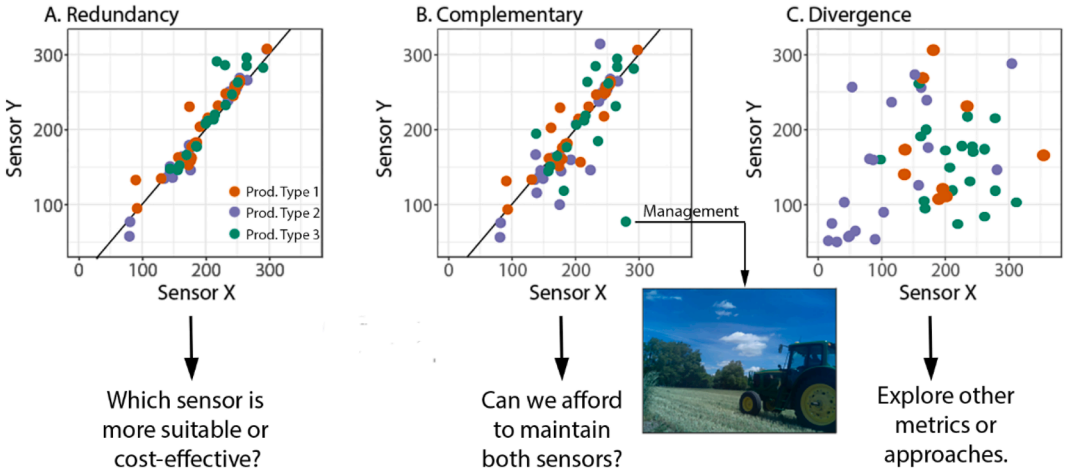

Fig. 9. Relationships in the metric assessment framework using data points from hypothetical, yet common situations in diverse production types (colored symbols). The framework is designed to help the user compare relative benefits of metrics from different sensors to meet specific management, monitoring or research goals. We define a redundant relationship where two sensors provide essentially the same information and interpretation (A); a complementary relationship where disagreements are well understood and can be integrated into decision making (B); and a divergent relationship where there is high disagreement between two sensors and the underlying cause is unknown (C).

g., one with a shorter revisit time than the 16-day revisit interval used here).

5.2. Key challenges identified across sensors and site types

While all four metrics examined can be used to address broadly similar questions in agroecosystems, they are, by design, built to capture different processes at different temporal and spatial scales. Our comparisons suggest some key principles to bear in mind when integrating sensor outputs across agricultural systems and scales.

5.2.1. Eddy covariance in remote agroecosystem landscapes

Eddy covariance flux tower measurements have provided numerous ecological insights (Baldocchi, 2020) and are commonly used to verify larger-scale modeling efforts (Jung et al., 2011, Zhang et al., 2015, Robinson et al., 2018, Badgley et al., 2019, Pei et al., 2020). By measuring biogeochemical fluxes at the ecosystem level they give a true phenological profile of soil and plant carbon fluxes processes within the tower footprint with high temporal frequency; even though energy balance closure problems at a site can affect the calculation of turbulent fluxes (Foken, 2008, Mauder et al., 2020). Instruments are expensive to establish, maintain and the data are difficult to process. Across the three production systems featured in this paper, EC towers were more common in cropland systems with heavily instrumented field and pasture-level operations. Establishing and maintaining EC towers can be cost-prohibitive for remote research sites.

In many western U.S. grazing systems, landscape elements based on dominant vegetation and soils are diverse and much of the terrain is remote (Browning et al., 2015). The combination of remote, diverse soil-landscape units makes the deployment and upkeep of EC instruments challenging. In the case of remote grazing lands, identifying sensors (e.g., PhenoCam) that yield metrics that are redundant or complementary to EC is beneficial. We found that annual production estimates from PhenoCams were better correlated with those from EC in grazing lands and moderately correlated in integrated and cropping systems. This finding suggests that less expensive PhenoCams might be a suitable proxy for EC towers in remote grazing systems. This solution is predicated on the availability of internet or cell phone network coverage. For example, PhenoCam and satellite data can be combined to provide a locally calibrated estimate of productivity (Wang et al., 2020).

5.2.2. Resolution of satellite revisit frequency

Earlier SOS, later EOS, and hence longer growing season length (GSL) estimated from the satellite platform was a consistent and unexpected finding. The general trend of increasing GSL from EC to PhenoCam to satellite (Fig. 3) could be explained by the size of the area over which the GPP and G_{CC} values are estimated. However, the pattern of longer GSL for sensors integrating over larger areas did not hold for grazing land sites that demonstrated the shortest mean GSL. This might be due to the larger range in latitude and precipitation for grazing land sites in this study (e.g., Fig. 1). We cannot attribute this effect to landscape heterogeneity, as the Shannon diversity index of surrounding land cover was poorly correlated with SOS differences among sensors although it did affect EOS estimates. Another possible explanation is that earlier onset dates were artifacts of the smoothing algorithm used in the upstream Landsat GPP dataset combined with a coarse 16-day temporal resolution.

We recognize that new satellite platforms provide higher spatial resolution and revisit frequencies than the Landsat GPP data product (Robinson et al., 2018) used in this study. A combination of increased spatial and temporal resolutions based on the fusion of Landsat and MODIS data, harmonized Landsat Sentinel-2 time series and future Landsat missions would be useful to evaluate in the future (Gao et al., 2015, Claverie et al., 2018; Bolton et al., 2020). We used the Landsat satellite GPP data product because it is the only GPP product available at a 30-m spatial resolution with CONUS coverage and also fully accessible through the Google Earth Engine platform. Another satellite platform that could potentially become a viable option for estimating productivity and phenological parameters is Planet Labs constellation, which has spatial resolutions ranging from 0.5 to 7 m and short (<16 days) revisit times (Moon et al., In Review). Agreements between research institutions and companies in the private sector, such as Planet Labs, are emerging and could allow for new options.

5.2.3. Tracking multiple growing seasons

The perennialization of cover is increasingly an objective in cropping systems (Wittwer et al., 2017). In the focal years of this study (2017 and 2018), a pattern of multiple growth cycles in one year was evident in integrated systems, but multiple cropping cycles per year is also a common aspect of crop-only systems, notably those associated with diversification objectives (Spiegal et al., 2018). Moreover, growing season length and phenological profiles are projected to increasingly shift with climate change (Hufkens et al., 2016). Detecting the start and end of the growing season from time series with multiple annual cycles is not a trivial task (Richardson et al., 2018a). We overcame this challenge by choosing the last EOS date for the calendar year, which may have over-estimated production by including fallow periods or time between first harvest and second growth in cropland systems. One solution to this problem would be to refine algorithms for identifying growing season start and end to improve estimates of annual production. For example we found better correspondence using a 50% threshold for our transition date extraction, and a suite of other methods are available which may be more appropriate in some scenarios (White et al., 2009).

5.3. Future directions

Linking on-the-ground agricultural management activities and sophisticated monitoring tools is among the greatest opportunities provided by the LTAR network. Future directions will explore the degree to which we can use sensor platforms to evaluate the impacts of management activities and climate change, including changes in the relationships among GPP, climate, and growing season length. Importantly, a priority will be assessing how those relationships can be used to predict the effects of management on sustainability outcomes such as soil health, carbon sequestration, food and fiber production, water conservation and overall human well-being.

Boundary organizations such as the Department of Interior Climate Adaptation Science Centers, NOAA Regional Integrated Science and Assessments and the USDA Climate Hub network operate at the interface of science to service, ultimately supporting management decisions. Climate Hubs translate scientific information and data into decision support tools, enabling producers and the USDA service agencies (e.g., National Resource Conservation Service, Farm Services Agency and Risk Management Agency) to support climate-informed decision-making. The USDA Climate Hubs are uniquely poised to interface with scientists and data networks to develop systems that enable economically viable agricultural management decisions relevant for cropland, grazing lands, and integrated systems in subtropical, temperate, and semi-arid regions that are represented in this analysis.

Despite the importance of management effects in agroecosystems, the collection and curation of detailed management data is notoriously difficult. In addition, complementing EC and satellite time series with regard to productivity and season length, ground-based PhenoCam photographs can help identify timing and nature of management events (e.g., dates of harvest, irrigation, grazing or fire) and even the effects of management on sustainability outcomes such as avian biodiversity. Cropping systems for site-years featured in this study constituted largely corn, soybean, and corn-soybean and cover crop rotations (Spiegal et al., 2018). Thus, there is potential for the PhenoCam network and automated image classification to develop datasets for management activities in croplands, and in grazing lands to some extent, that can be used as inputs for models and context for monitoring (Lombardozzi et al.,

2020). Understanding how growing season metrics correlate or vary across platforms is foundational to informed decision-making for technological investment. We offer the metric assessment framework designed to optimize instrumentation selection for monitoring, modeling, and forecasting ecosystem functioning with the ultimate goal of informing decisions to meet sustainability goals in agriculture.

CRediT authorship contribution statement

Dawn M. Browning: Conceptualization, Validation, Investigation, Data curation, Writing - original draft, Writing - review & editing, Supervision. **Eric S. Russell:** Methodology, Software, Validation, Data curation, Writing - original draft, Visualization. **Guillermo E. Ponce-Campos:** Methodology, Resources, Writing - original draft, Writing - review & editing. **Nicole Kaplan:** Methodology, Software, Validation, Data curation. **Andrew D. Richardson:** Conceptualization, Validation, Writing - review & editing, Funding acquisition. **Bijan Seyednasrollah:** Conceptualization, Software, Validation, Investigation, Writing - original draft. **Sheri Spiegal:** Conceptualization, Writing - original draft, Writing - review & editing. **Nicanor Saliendra:** Conceptualization, Validation, Data curation, Writing - review & editing. **Joseph G. Alfieri:** Validation, Data curation, Writing - review & editing. **John Baker:** Validation, Data curation, Writing - review & editing. **Carl Bernacchi:** Validation, Data curation, Writing - review & editing. **Brandon T. Bestelmeyer:** Funding acquisition, Writing - review & editing. **David Bosch:** Validation, Data curation, Writing - review & editing. **Elizabeth H. Boughton:** Validation, Data curation, Writing - review & editing. **Raoul K. Boughton:** Validation, Data curation, Writing - review & editing. **Pat Clark:** Validation, Data curation, Writing - review & editing. **Gerald Flerchinger:** Validation, Data curation, Writing - review & editing. **Nuria Gomez-Casanovas:** Validation, Data curation, Writing - review & editing. **Sarah Goslee:** Software, Validation, Data curation, Writing - review & editing. **Nick M. Haddad:** Conceptualization, Writing - original draft. **David Hoover:** Conceptualization, Validation, Data curation, Writing - original draft, Writing - review & editing. **Abdullah Jaradat:** Validation, Data curation, Writing - review & editing. **Marguerite Mauritz:** Validation, Investigation, Data curation, Writing - review & editing, Visualization. **Gregory W. McCarty:** Data curation. **Gretchen R. Miller:** Validation, Data curation, Writing - review & editing. **John Sadler:** Validation, Data curation, Writing - review & editing. **Amartya Saha:** Validation, Data curation, Writing - review & editing. **Russell L. Scott:** Conceptualization, Validation, Data curation, Writing - review & editing. **Andrew Suyker:** Validation, Data curation, Writing - review & editing. **Craig Tweedie:** Funding acquisition, Writing - review & editing. **Jeffrey D. Wood:** Validation, Data curation, Writing - review & editing. **Xukai Zhang:** Data curation, Writing - review & editing. **Shawn D. Taylor:** Methodology, Software, Validation, Formal analysis, Investigation, Data curation, Writing - original draft, Writing - review & editing, Visualization.

Declaration of Competing Interest

The authors declare that they have no known competing financial interests or personal relationships that could have appeared to influence the work reported in this paper.

Acknowledgments

This research was a contribution from the Long-Term Agroecosystem Research (LTAR) network. LTAR is supported by the United States Department of Agriculture. The authors acknowledge the USDA Agricultural Research Service (ARS) Big Data Initiative and SCINet high performance computing resources (https://scinet.usda.gov) made available for conducting the research reported in this paper. Support for this research was also provided by the NSF Long-term Ecological Research Program (LTER; DEB 1832042) at the Kellogg Biological Station and LTER-VI at the Jornada Basin LTER (DEB 1235828) and from NSF CREST Phase II: Cyber-ShARE Center of Excellence (NSF 1242122; NSF 0734825). We acknowledge valuable suggestions from three anonymous reviewers and E. Elias and R. Wu who contributed to the graphical abstract.

We thank our many collaborators, including site PIs and technicians, for their efforts in support of PhenoCam. The development of PhenoCam Network has been funded by the Northeastern States Research Cooperative, NSF's Macrosystems Biology program (awards EF-1065029 and EF-1702697), and DOE's Regional and Global Climate Modeling program (award DE-SC0016011). AmeriFlux is sponsored by the U.S. Department of Energy's Office of Science.

Specifically, we acknowledge the efforts of the following site research and support personnel: Earl Keel, David Smith, Dan Arthur, Ruben Baca, Jeff Gonet, Lou Saporito, Steve Van Vactor, Bryan Carlson, Patrick O'Keeffe, Shefali Azad, Vivienne Sclater, Maria Silveira, Binayak Mohanty, Georgianne Moore, Doug Smith, Deanroy Mbabazi, Chris Wente and Steve Wagner.

Appendix A. Supplementary data

Supplementary data to this article can be found online at https://doi.org/10.1016/j.ecolind.2021.108147.

References

Abraha, M., Chen, J., Chu, H., Zenone, T., John, R., Yahn-Jauh, S., Hamilton, S.K., Philip Robertson, G., 2015. Evapotranspiration of annual and perennial biofuel crops in a variable climate. GCB Bioenergy 7 (6), 1344–1356. https://doi.org/10.1111/gcbb.12239.

Anderson-Teixeira, K.J., Delong, J.P., Fox, A.M., Brese, D.A., Litvak, M.E., 2011. Differential responses of production and respiration to temperature and moisture drive the carbon balance across a climatic gradient in New Mexico. Glob. Chang. Biol. 17, 410–424. https://doi.org/10.1111/j.1365-2486.2010.02269.x.

Aubinet, Marc, Timo Vesala, and Dario Papale, eds. 2012. Eddy Covariance: A Practical Guide to Measurement and Data Analysis. Dordrecht: Springer Netherlands. https://doi.org/10.1007/978-94-007-2351-1.

Badgley, G., Anderegg, L.D.L., Berry, J.A., Field, C.B., 2019. Terrestrial gross primary production: using NIR V to scale from site to globe. Glob. Change Biol. 25 (11), 3731–3740. https://doi.org/10.1111/gcb.14729.

Baffaut, Claire, John M Baker, Joel A Biederman, David D Bosch, Erin S. Brooks, Anthony R Buda, Eleonora M Demaria, et al. 2020. Comparative Analysis of Water Budgets across the U.S. Long-Term Agroecosystem Research Network. J. Hydrol., May, 125021. https://doi.org/10.1016/j.jhydrol.2020.125021.

Baldocchi, D.D., 2020. How Eddy covariance flux measurements have contributed to our understanding of global change biology. Glob. Change Biol. 26 (1), 242–260. https://doi.org/10.1111/gcb.v26.110.1111/gcb.14807.

Balzarolo, M., Vicca, S., Nguy-Robertson, A.L., Bonal, D., Elbers, J.A., Fu, Y.H., Grünwald, T., Horemans, J.A., Papale, D., Peñuelas, J., Suyker, A., Veroustraete, F., 2016. Matching the phenology of net ecosystem exchange and vegetation indices estimated with MODIS and FLUXNET in-situ observations. Remote Sens. Environ. 174, 290–300. https://doi.org/10.1016/j.rse.2015.12.017.

Belsky, A.J., 1986. Does herbivory benefit plants? a review of the evidence. Am. Nat. 127 (6), 870–892. https://doi.org/10.1086/284531.

Biederman, J.A., Scott, R.L., Bell, T.W., Bowling, D.R., Dore, S., Garatuza-Payan, J., Kolb, T.E., et al., 2017. CO2 Exchange and evapotranspiration across dryland ecosystems of Southwestern North America. Glob. Change Biol. 23 (10), 4204–4221. https://doi.org/10.1111/gcb.13686.

Bolton, D.K., Gray, J.M., Melaas, E.K., Moon, M., Eklundh, L., Friedl, M.A., 2020. Continental-scale land surface phenology from harmonized landsat 8 and sentinel-2 imagery. Remote Sens. Environ. 240 (April), 111685 https://doi.org/10.1016/j.rse.2020.111685.

Briske, D.D., Derner, J.D., Brown, J.R., Fuhlendorf, S.D., Teague, W.R., Havstad, K.M., Gillen, R.L., Ash, A.J., Willms, W.D., 2008. Rotational grazing on rangelands: reconciliation of perception and experimental evidence. Rangeland Ecol. Manage. 61 (1), 3–17. https://doi.org/10.2111/06-159R.1.

Browning, D.M., Karl, J.W., Morin, D., Richardson, A.D., Tweedie, C.E., 2017. Phenocams bridge the gap between field and satellite observations in an arid grassland ecosystem. Remote Sensing 9 (10), 1071. https://doi.org/10.3390/rs9101071.

Browning, D.M., Rango, A., Karl, J.W., Laney, C.M., Vivoni, E.R., Tweedie, C.E., 2015. Emerging technological and cultural shifts advancing drylands research and management. Front. Ecol. Environ. 13 (1), 52–60. https://doi.org/10.1890/140161.

Buitenwerf, R., Rose, L., Higgins, S.I., 2015. Three Decades of multi-dimensional change in global leaf phenology. Nat. Clim. Change 5 (4), 364–368. https://doi.org/10.1038/nclimate2533.

Burba, G., 2013. Eddy Covariance Method for Scientific, Industrial, Agricultural and Regulatory Applications: A Field Book on Measuring Ecosystem Gas Exchange and Areal Emission Rates. LI-Cor Biosciences.

Butterfield, H.S., Malmström, C.M., 2009. The effects of phenology on indirect measures of aboveground biomass in annual grasses. Int. J. Remote Sens. 30 (12), 3133–3146. https://doi.org/10.1080/01431160802558774.

Chu, H., Luo, X., Ouyang, Z., Chan, W.S., Dengel, S., Biraud, S.C., Torn, M.S., Metzger, S., Kumar, J., Arain, M.A., Arkebauer, T.J., Baldocchi, D., Bernacchi, C., Billesbach, D., Black, T.A., Blanken, P.D., Bohrer, G., Bracho, R., Brown, S., Brunsell, N.A., Chen, J., Chen, X., Clark, K., Desai, A.R., Duman, T., Durden, D., Fares, S., Forbrich, I., Gamon, J.A., Gough, C.M., Griffis, T., Helbig, M., Hollinger, D., Humphreys, E., Ikawa, H., Iwata, H., Ju, Y., Knowles, J.F., Knox, S.H., Kobayashi, H., Kolb, T., Law, B., Lee, X., Litvak, M., Liu, H., Munger, J.W., Noormets, A., Novick, K., Oberbauer, S.F., Oechel, W., Oikawa, P., Papuga, S.A., Pendall, E., Prajapati, P., Prueger, J., Quinton, W.L., Richardson, A.D., Russell, E.S., Scott, R.L., Starr, G., Staebler, R., Stoy, P.C., Stuart-Haëntjens, E., Sonnentag, O., Sullivan, R.C., Suyker, A., Ueyama, M., Vargas, R., Wood, J.D., Zona, D., 2021. Representativeness of Eddy-covariance flux footprints for areas surrounding AmeriFlux sites. Agric. For. Meteorol. 301-302, 108350. https://doi.org/10.1016/j.agrformet.2021.108350.

Claverie, M., Junchang, J.u., Masek, J.G., Dungan, J.L., Vermote, E.F., Roger, J.-C., Skakun, S.V., Justice, C., 2018. The harmonized landsat and sentinel-2 surface reflectance data set. Remote Sens. Environ. 219 (December), 145–161. https://doi.org/10.1016/j.rse.2018.09.002.

Delpierre, N., Vitasse, Y., Chuine, I., Guillemot, J., Bazot, S., Rutishauser, T., Rathgeber, C.B.K., 2016. Temperate and boreal forest tree phenology: from organ-scale processes to terrestrial ecosystem models. Annals of Forest Science 73 (1), 5–25. https://doi.org/10.1007/s13595-015-0477-6.

Fan, L., Ketzer, B., Liu, H., Bernhofer, C., 2011. Grazing effects on seasonal dynamics and interannual variabilities of spectral reflectance in semi-arid grassland in Inner Mongolia. Plant Soil 340 (1–2), 169–180. https://doi.org/10.1007/s11104-010-0448-5.

Flerchinger, G.N., Fellows, A.W., Seyfried, M.S., Clark, P.E., Lohse, K.A., 2020. Water and carbon fluxes along an elevational gradient in a sagebrush ecosystem. Ecosystems 23 (2), 246–263. https://doi.org/10.1007/s10021-019-00400-x.

Foken, T., 2008. The energy balance closure problem: an overview. Ecol. Appl. 18 (6), 1351–1367. https://doi.org/10.1890/06-0922.1.

Frank, D.A., McNaughton, S.J., 1993. Evidence for the promotion of aboveground grassland production by native large herbivores in yellowstone national park. Oecologia 96 (2), 157–161. https://doi.org/10.1007/BF00317727.

Fritz, Steffen, Linda See, Juan Carlos Laso Bayas, François Waldner, Damien Jacques, Inbal Becker-Reshef, Alyssa Whitcraft, et al. 2019. A comparison of global agricultural monitoring systems and current gaps. Agricultural Systems 168 (December 2017): 258–72. https://doi.org/10.1016/j.agsy.2018.05.010.

Gao, F., Hilker, T., Zhu, X., Anderson, M., Masek, J., Wang, P., Yang, Y., 2015. Fusing landsat and MODIS data for vegetation monitoring. IEEE Geosci. Remote Sens. Mag. 3 (3), 47–60. https://doi.org/10.1109/MGRS.2015.2434351.

Gao, Xueyuan, Shunlin Liang, Bin He. 2019. Detected global agricultural greening from satellite data. Agric. Forest Meteorol. 276–277 (October 2018): 107652. https://doi.org/10.1016/j.agrformet.2019.107652.

Garonna, I., de Jong, R., Schaepman, M.E., 2016. Variability and evolution of global land surface phenology over the past three decades (1982–2012). Glob. Change Biol. 22 (4), 1456–1468. https://doi.org/10.1111/gcb.2016.22.issue-410.1111/gcb.13168.

Gomez-Casanovas, N., DeLucia, N.J., DeLucia, E.H., Blanc-Betes, E., Boughton, E.H., Sparks, J., Bernacchi, C.J., 2020. Seasonal controls of CO 2 and CH 4 dynamics in a temporarily flooded subtropical wetland. J. Geophys. Res. Biogeosci. 125 (3) https://doi.org/10.1029/2019JG005257.

Griffis, T.J., Baker, J.M., Zhang, J., 2005. Seasonal dynamics and partitioning of isotopic CO2 exchange in a C3/C4 managed ecosystem. Agric. For. Meteorol. 132 (1–2), 1–19. https://doi.org/10.1016/j.agrformet.2005.06.005.

Hank, T., Bach, H., Mauser, W., 2015. Using a remote sensing-supported hydro-agroecological model for field-scale simulation of heterogeneous crop growth and yield: application for wheat in central europe. Remote Sens. 7 (4), 3934–3965. https://doi.org/10.3390/rs70403934.

Hufkens, K., Keenan, T.F., Flanagan, L.B., Scott, R.L., Bernacchi, C.J., Joo, E., Brunsell, N. A., Verfaillie, J., Richardson, A.D., 2016. Productivity of North American grasslands is increased under future climate scenarios despite rising aridity. Nat. Clim. Change 6 (7), 710–714. https://doi.org/10.1038/nclimate2942.

Hufkens, K., Melaas, E.K., Mann, M.L., Foster, T., Ceballos, F., Robles, M., Kramer, B., 2019. Monitoring crop phenology using a smartphone based near-surface remote sensing approach. Agric. For. Meteorol. 265 (February), 327–337. https://doi.org/10.1016/j.agrformet.2018.11.002.

Jung, M., Reichstein, M., Margolis, H.A., Cescatti, A., Richardson, A.D., Arain, M.A., Arneth, A., Bernhofer, C., Bonal, D., Chen, J., Gianelle, D., Gobron, N., Kiely, G., Kutsch, W., Lasslop, G., Law, B.E., Lindroth, A., Merbold, L., Montagnani, L., Moors, E.J., Papale, D., Sottocornola, M., Vaccari, F., Williams, C., 2011. Global patterns of land-atmosphere fluxes of carbon dioxide, latent heat, and sensible heat derived from eddy covariance, satellite, and meteorological observations. J. Geophys. Res. 116 https://doi.org/10.1029/2010JG001566.

Keller, M., Schimel, D.S., William Hargrove, W., Hoffman, F.M., 2008. A Continental Strategy For The National Ecological Observatory Network. Ecol. Soc. Am. 282–284 https://doi.org/10.1890/1540-9295(2008)6[282:ACSFTN]2.0.CO;2.

Kleinman, P.J.A., Spiegal, S., Rigby, J.R., Goslee, S.C., Baker, J.M., Bestelmeyer, B.T., Boughton, R.K., Bryant, R.B., Cavigelli, M.A., Derner, J.D., Duncan, E.W., Goodrich, D.C., Huggins, D.R., King, K.W., Liebig, M.A., Locke, M.A., Mirsky, S.B., Moglen, G.E., Moorman, T.B., Pierson, F.B., Robertson, G.P., Sadler, E.J., Shortle, J. S., Steiner, J.L., Strickland, T.C., Swain, H.M., Tsegaye, T., Williams, M.R., Walthall, C.L., 2018. Advancing the sustainability of US agriculture through long-term research. J. Environ. Qual. 47 (6), 1412–1425. https://doi.org/10.2134/jeq2018.05.0171.

Klosterman, S.T., Hufkens, K., Gray, J.M., Melaas, E., Sonnentag, O., Lavine, I., Mitchell, L., Norman, R., Friedl, M.A., Richardson, A.D., 2014. Evaluating remote sensing of deciduous forest phenology at multiple spatial scales using phenocam imagery. Biogeosciences 11 (16), 4305–4320. https://doi.org/10.5194/bg-11-4305-2014.

Knapp, Alan K., Melinda D. Smith, Sarah E. Hobbie, Scott L. Collins, Timothy J. Fahey, Gretchen J. A. Hansen, Douglas A. Landis, et al. 2012. Past, present, and future roles of long-term experiments in the LTER Network. BioScience 62 (4): 377–89. https://doi.org/10.1525/bio.2012.62.4.9.

Kukal, M.S., Irmak, S., 2018. U.S. Agro-Climate in 20th century: growing degree days, first and last frost, growing season length, and impacts on crop yields. Sci. Rep. 8 (1), 6977. https://doi.org/10.1038/s41598-018-25212-2.

Li, F., Kustas, W.P., Anderson, M.C., Prueger, J.H., Scott, R.L., 2008. Effect of remote sensing spatial resolution on interpreting tower-based flux observations. Remote Sens. Environ. 112 (2), 337–349. https://doi.org/10.1016/j.rse.2006.11.032.

Lombardozzi, Danica L., Yaqiong Lu, Peter J. Lawrence, David M. Lawrence, Sean Swenson, Keith W. Oleson, William R. Wieder, Elizabeth A. Ainsworth. 2020. Simulating Agriculture in the Community Land Model Version 5. J. Geophys. Res.: Biogeosciences, June, 0–3. https://doi.org/10.1029/2019JG005529.

Mauder, M., Foken, T., Cuxart, J., 2020. Surface-energy-balance closure over land: a review. Boundary-Layer Meteorol. 177 (2-3), 395–426. https://doi.org/10.1007/s10546-020-00529-6.

Metzger, Stefan, Edward Ayres, David Durden, Christopher Florian, Robert Lee, Claire Lunch, Hongyan Luo, et al. 2019. From NEON Field Sites to Data Portal: A community resource for surface–atmosphere research comes online. Bull. Am. Meteorol. Soc. 100 (11): 2305–25. https://doi.org/10.1175/BAMS-D-17-0307.1.

Milchunas, D.G., Lauenroth, W.K., 1993. Quantitative effects of grazing on vegetation and soils over a global range of environments. Ecol. Monogr. 63 (4), 327–366. https://doi.org/10.2307/2937150.

Milliman, T, B Seyednasrollah, A M Young, K Hufkens, M A Friedl, S Frolking, A D Richardson, et al. 2019. "PhenoCam Dataset v2.0: Digital Camera Imagery from the PhenoCam Network, 2000-2018." ORNL Distributed Active Archive Center. https://doi.org/10.3334/ORNLDAAC/1689.

Moon, M., Richardson, A. D. & Friedl, M. A. (In Review). Multiscale Assessment of Land Surface Phenology from Harmonized Landsat 8 and Sentinel-2, PlanetScope, and Phenocam Imagery. Remote Sensing of Environment.

Norris, J.R., Walker, J.J., 2020. Solar and sensor geometry, not vegetation response, drive satellite NDVI phenology in widespread ecosystems of the Western United States. Remote Sens. Environ. 249 (November), 112013 https://doi.org/10.1016/j.rse.2020.112013.

Novick, K.A., Biederman, J.A., Desai, A.R., Litvak, M.E., Moore, D.J.P., Scott, R.L., Torn, M.S., 2018. The AmeriFlux network: a coalition of the willing. Agric. For. Meteorol. 249 (February), 444–456. https://doi.org/10.1016/j.agrformet.2017.10.009.

Pei, Y., Dong, J., Zhang, Y., Yang, J., Zhang, Y., Jiang, C., Xiao, X., 2020. Performance of four state-of-the-Art GPP Products (VPM, MOD17, BESS and PML) for Grasslands in Drought Years. Ecol. Inf. 56 (March), 101052 https://doi.org/10.1016/j.ecoinf.2020.101052.

PRISM Climate Group. 2004. Oregon State University. http://prism.oregonsate.edu.

Reichstein, M., Falge, E., Baldocchi, D., Papale, D., Aubinet, M., Berbigier, P., Bernhofer, C., Buchmann, N., Gilmanov, T., Granier, A., Grunwald, T., Havrankova, K., Ilvesniemi, H., Janous, D., Knohl, A., Laurila, T., Lohila, A., Loustau, D., Matteucci, G., Meyers, T., Miglietta, F., Ourcival, J.-M., Pumpanen, J., Rambal, S., Rotenberg, E., Sanz, M., Tenhunen, J., Seufert, G., Vaccari, F., Vesala, T., Yakir, D., Valentini, R., 2005. On the separation of net ecosystem exchange into assimilation and ecosystem respiration: review and improved algorithm. Glob. Change Biol. 11 (9), 1424–1439. https://doi.org/10.1111/gcb.2005.11.issue-910.1111/j.1365-2486.2005.001002.x.

Reinermann, S., Asam, S., Kuenzer, C., 2020. Remote sensing of grassland production and management—a review. Remote Sensing 12 (12), 1949. https://doi.org/10.3390/rs12121949.

Richardson, A.D., Hufkens, K., Milliman, T., Aubrecht, D.M., Chen, M., Gray, J.M., Johnston, M.R., Keenan, T.F., Klosterman, S.T., Kosmala, M., Melaas, E.K., Friedl, M. A., Frolking, S., 2018a. Tracking vegetation phenology across diverse north american biomes using PhenoCam imagery. Sci. Data 5 (1). https://doi.org/10.1038/sdata.2018.28.

Richardson, A.D., Hufkens, K., Milliman, T., Frolking, S., 2018b. Intercomparison of phenological transition dates derived from the PhenoCam Dataset V1.0 and MODIS satellite remote sensing. Sci. Rep. 8 (1), 5679. https://doi.org/10.1038/s41598-018-23804-6.

Robinson, N., Allred, B., Jones, M., Moreno, A., Kimball, J., Naugle, D., Erickson, T., Richardson, A., 2017. A Dynamic landsat derived normalized difference vegetation index (NDVI) product for the conterminous United States. Remote Sens. 9 (8), 863. https://doi.org/10.3390/rs9080863.

Robinson, Nathaniel P., Brady W. Allred, William K. Smith, Matthew O. Jones, Alvaro Moreno, Tyler A. Erickson, David E. Naugle, and Steven W. Running. 2018. Terrestrial Primary Production for the Conterminous United States Derived from Landsat 30 m and MODIS 250 M." Edited by Nathalie Pettorelli and Jose Paruelo. Remote Sens. Ecol. Conserv. 4 (3): 264–80. https://doi.org/10.1002/rse2.74.

Running, S.N.W., Nemani, R.R., Heinsch, F.A.N.N., Zhao, M., Reeves, M., Hashimoto, H., 2004. A continuous satellite-derived measure of global terrestrial primary production. Bioscience 54 (6). https://doi.org/10.1641/0006-3568(2004)054[0547:ACSMOG]2.0.CO;2.

Russell, E.S., Dziekan, V., Chi, J., Waldo, S., Pressley, S.N., O'Keeffe, P., Lamb, B.K., 2019. Adjustment of CO2 flux measurements due to the bias in the EC150 infrared gas analyzer. Agric. For. Meteorol. 276–277 (October), 107593 https://doi.org/10.1016/j.agrformet.2019.05.024.

Saliendra, N.Z., Liebig, M.A., Kronberg, S.L., 2018. Carbon Use efficiency of hayed alfalfa and grass pastures in a semiarid environment. Ecosphere 9 (3), e02147. https://doi.org/10.1002/ecs2.2147.

Scott, R.L., Biederman, J.A., Hamerlynck, E.P., Barron-Gafford, G.A., 2015. The carbon balance pivot point of southwestern U.S. Semiarid Ecosystems: insights from the 21st century drought. J. Geophys. Res. Biogeosci. 120 (12), 2612–2624. https://doi.org/10.1002/2015JG003181.

Seo, B., Lee, J., Lee, K.-D., Hong, S., Kang, S., 2019. Improving remotely-sensed crop monitoring by NDVI-based crop phenology estimators for corn and soybeans in Iowa and Illinois, USA. Field Crops Research 238 (May), 113–128. https://doi.org/10.1016/j.fcr.2019.03.015.

Seyednasrollah, B., Milliman, T., Richardson, A.D., 2019a. Data extraction from digital repeat photography using XROI: an Interactive Framework to Facilitate the Process. ISPRS J. Photogramm. Remote Sens. 152 (June), 132–144. https://doi.org/10.1016/j.isprsjprs.2019.04.009.

Seyednasrollah, B., Young, A.M., Hufkens, K., Milliman, T., Friedl, M.A., Frolking, S., Richardson, A.D., 2019b. Tracking vegetation phenology across diverse biomes using version 2.0 of the PhenoCam dataset. Sci. Data 6 (1), 222. https://doi.org/10.1038/s41597-019-0229-9.

Seyednasrollah, B, A M Young, K Hufkens, T Milliman, M A Friedl, S Frolking, A D Richardson, et al. 2019c. PhenoCam Dataset v2.0: Vegetation Phenology from Digital Camera Imagery, 2000-2018. ORNL Distributed Active Archive Center. https://doi.org/10.3334/ORNLDAAC/1674.

Shannon, C.E., 1948. A mathematical theory of communication. Bell System Techn. J. 27 (3), 379–423.

Skinner, R.H., 2008. High biomass removal limits carbon sequestration potential of mature temperate pastures. J. Environ. Qual. 37 (4), 1319–1326. https://doi.org/10.2134/jeq2007.0263.

Smith, W.K., Dannenberg, M.P., Yan, D., Herrmann, S., Barnes, M.L., Barron-Gafford, G. A., Biederman, J.A., Ferrenberg, S., Fox, A.M., Hudson, A., Knowles, J.F., MacBean, N., Moore, D.J.P., Nagler, P.L., Reed, S.C., Rutherford, W.A., Scott, R.L., Wang, X., Yang, J., 2019. Remote sensing of dryland ecosystem structure and function: progress, challenges, and opportunities. Remote Sens. Environ. 233, 111401. https://doi.org/10.1016/j.rse.2019.111401.

Spiegal, S., Bestelmeyer, B.T., Archer, D.W., Augustine, D.J., Boughton, E.H., Boughton, R.K., Cavigelli, M.A., Clark, P.E., Derner, J.D., Duncan, E.W., Hapeman, C. J., Harmel, R.D., Heilman, P., Holly, M.A., Huggins, D.R., King, K., Kleinman, P.J.A., Liebig, M.A., Locke, M.A., McCarty, G.W., Millar, N., Mirsky, S.B., Moorman, T.B., Pierson, F.B., Rigby, J.R., Robertson, G.P., Steiner, J.L., Strickland, T.C., Swain, H. M., Wienhold, B.J., Wulfhorst, J.D., Yost, M.A., Walthall, C.L., 2018. Evaluating Strategies for Sustainable Intensification of US Agriculture through the Long-Term Agroecosystem Research Network. Environ. Res. Lett. 13 (3), 034031. https://doi.org/10.1088/1748-9326/aaa779.

Suyker, A.E., Verma, S.B., Burba, G.G., Arkebauer, T.J., 2005. Gross primary production and ecosystem respiration of irrigated maize and irrigated soybean during a growing season. Agric. For. Meteorol. 131 (3–4), 180–190. https://doi.org/10.1016/j.agrformet.2005.05.007.

Toomey, M., Friedl, M.A., Frolking, S., Hufkens, K., Klosterman, S., Sonnentag, O., Baldocchi, D.D., Bernacchi, C.J., Biraud, S.C., Bohrer, G., Brzostek, E., Burns, S.P., Coursolle, C., Hollinger, D.Y., Margolis, H.A., McCaughey, H., Monson, R.K., Munger, J.W., Pallardy, S., Phillips, R.P., Torn, M.S., Wharton, S., Zeri, M., Richardson, A.D., 2015. Greenness indices from digital cameras predict the timing and seasonal dynamics of canopy-scale photosynthesis. Ecol. Appl. 25 (1), 99–115. https://doi.org/10.1890/14-0005.110.1890/14-0005.1.sm.

Tracy, B.F., Foster, J.L., Butler, T.J., Islam, M.A., Toledo, D., Vendramini, J.M.B., 2018. Resilience in forage and grazinglands. Crop Sci. 58 (1), 31–42. https://doi.org/10.2135/cropsci2017.05.0317.

Turner, M.G., 1989. Landscape Ecology: the effect of pattern on process. Annu. Rev. Ecol. Syst. 20 (1), 171–197. https://doi.org/10.1146/annurev.es.20.110189.001131.

USDA National Agricultural Statistics Service Cropland Data Layer. 2021. Published crop-specific data layer [Online]. Available at https://nassgeodata.gmu.edu/CropScape/ (accessed March 21, 2021). USDA-NASS, Washington, DC.

Vickers, D., Mahrt, L., 1997. Quality control and flux sampling problems for tower and aircraft data. J. Atmos. Oceanic Technol. 14 (3), 512–526. https://doi.org/10.1175/1520-0426(1997)014<0512:QCAFSP>2.0.CO;2.

Wang, H., Jia, G., Epstein, H.E., Zhao, H., Zhang, A., 2020. Integrating a PhenoCam-derived vegetation index into a light use efficiency model to estimate daily gross primary production in a semi-arid grassland. Agric. For. Meteorol. 288–289 (July), 107983 https://doi.org/10.1016/j.agrformet.2020.107983.

Weiss, M., Jacob, F., Duveiller, G., 2020. Remote sensing for agricultural applications: a meta-review. Remote Sens. Environ. 236 (January), 111402 https://doi.org/10.1016/j.rse.2019.111402.

White, Michael A., Kirsten M. de Beurs, Kamel Didan, David W. Inouye, Andrew D. Richardson, Olaf P. Jensen, John O'Keefe, et al. 2009. Intercomparison, interpretation, and assessment of spring phenology in North America estimated from remote sensing for 1982-2006. Global Change Biol. 15 (10): 2335–59. https://doi.org/10.1111/j.1365-2486.2009.01910.x.

Wilmer, H., Derner, J.D., Fernández-Giménez, M.E., Briske, D.D., Augustine, D.J., Porensky, L.M., 2018. Collaborative adaptive rangeland management fosters management-science partnerships. Rangeland Ecol. Manage. 71 (5), 646–657. https://doi.org/10.1016/j.rama.2017.07.008.

Wittwer, R.A., Dorn, B., Jossi, W., van der Heijden, M.G.A., 2017. Cover crops support ecological intensification of arable cropping systems. Sci. Rep. 7 (1), 41911. https://doi.org/10.1038/srep41911.

Wood, J.D., Sadler, E.J., Fox, N.I., Greer, S.T., Gu, L., Guinan, P.E., Lupo, A.R., Market, P. S., Rochette, S.M., Speck, A., White, L.D., 2019. Land-atmosphere responses to a total solar eclipse in three ecosystems with contrasting structure and physiology. J. Geophys. Res.: Atmospheres 124 (2), 530–543. https://doi.org/10.1029/2018JD029630.

Wu, C., Peng, D., Soudani, K., Siebicke, L., Gough, C.M., Arain, M.A., Bohrer, G., Lafleur, P.M., Peichl, M., Gonsamo, A., Xu, S., Fang, B., Ge, Q., 2017. Land surface phenology derived from normalized difference vegetation index (NDVI) at Global FLUXNET Sites. Agric. For. Meteorol. 233, 171–182. https://doi.org/10.1016/j.agrformet.2016.11.193.

Wutzler, T., Lucas-Moffat, A., Migliavacca, M., Knauer, J., Sickel, K., Šigut, L., Menzer, O., Reichstein, M., 2018. Basic and extensible post-processing of eddy covariance flux data with REddyProc. Biogeosciences 15 (16), 5015–5030. https://doi.org/10.5194/bg-15-5015-2018.

Yan, D., R.L. Scott, D.J.P. Moore, J.A. Biederman, W.K. Smith. 2019. Understanding the Relationship between Vegetation greenness and productivity across dryland ecosystems through the integration of PhenoCam, Satellite, and Eddy Covariance Data. Remote Sens. Environ. 223 (March 2018): 50–62. https://doi.org/10.1016/j.rse.2018.12.029.

Zhang, L.-X., Zhou, D.-C., Fan, J.-W., Zhong-Min, H., 2015. Comparison of four light use efficiency models for estimating terrestrial gross primary production. Ecol. Model. 300 (March), 30–39. https://doi.org/10.1016/j.ecolmodel.2015.01.001.

Further reading

Watson, Christopher J., Natalia Restrepo-Coupe, and Alfredo R. Huete. 2019. Multi-scale phenology of temperate grasslands: improving monitoring and management with near-surface phenocams. Front. Environ. Sci. 7 (February). https://doi.org/10.3389/fenvs.2019.00014.

8. Supplemental Information

Supplemental Table 1 is in the attached pdf.

Supplemental Table 2: Average start of season (SOS), end of season (EOS) and growing season length (GSL) of the three LTAR production systems as measured by the four metrics from 2017 and 2018 growing seasons. Parenthesis represent 1 standard deviation.

Production System	**sensor**	**No. site years**	**SOS (DOY)**	**EOS (DOY)**	**GLS (No. Days)**
cropland	EC GPP	23	160.3 (25.7)	234.1 (24.3)	73.8 (38.1)
cropland	PhenoCam G_{CC}	33	147.6 (30.4)	251.5 (34.6)	104.9 (40.3)
cropland	Satellite GPP	34	103.2 (26.5)	259 (24.9)	155.8 (23.3)
cropland	Satellite NDVI	34	108.5 (35.5)	286 (38.6)	177.4 (49.6)
grazing	EC GPP	22	128.7 (59.9)	264.2 (62.9)	135.5 (105.4)
grazing	PhenoCam G_{CC}	15	155 (42)	242.9 (44.6)	90.9 (59.3)
grazing	Satellite GPP	24	85.3 (44.1)	285.6 (38.2)	200.3 (55.3)
grazing	Satellite NDVI	22	106.8 (68.5)	313.1 (40.1)	206.3 (89.1)
integrated	EC GPP	6	138.8 (48)	253.5 (14)	114.7 (58.2)
integrated	PhenoCam G_{CC}	7	123.7 (55.4)	270 (18.7)	142 (59.3)
integrated	Satellite GPP	10	78.7 (38.8)	293.5 (29.9)	214.8 (59.5)
integrated	Satellite NDVI	10	84.4 (61.2)	313 (35.9)	228.6 (91.6)

Figure S1: Map of network locations used in the analysis. Point shapes represent the three networks: LTAR, NEON and LTER. Point color respects the three agroecosystem types: cropland, grazing and integrated sites. For the locations with multiple flux towers, the location names are followed by the numbers of flux towers or sites (*n*). Colored polygons represent estimated regional inference spaces for the 18 LTAR sites as defined in Spiegal et al. (2018). Projection: Albers equal area conic.

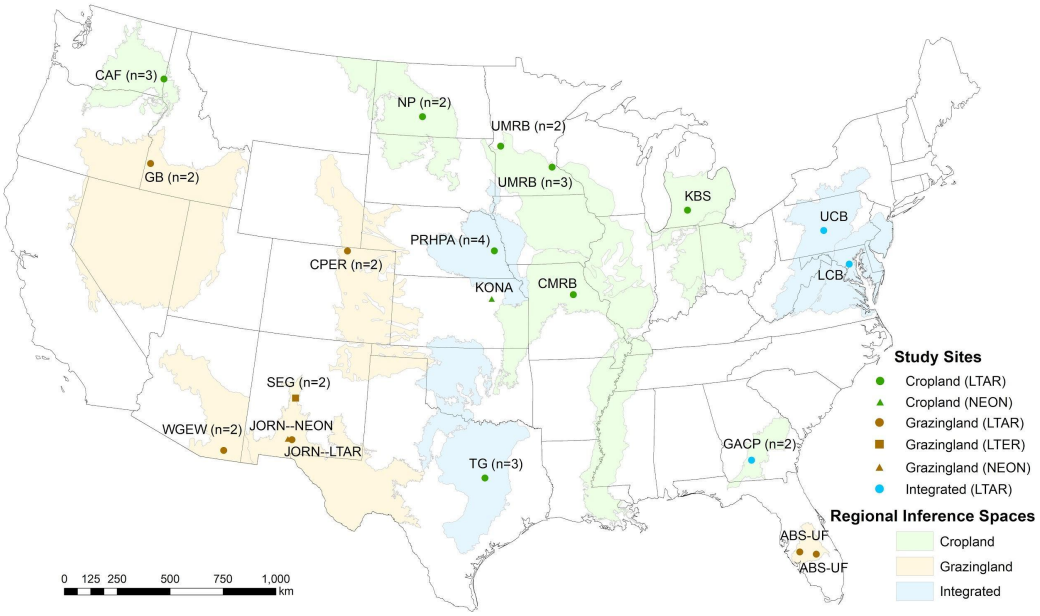

Supplemental Table 1: Details for 34 sites used in the analysis. Cited references are included in Table 1.

LTAR Site	EC Tower Name	Phenocam	LTAR Site Type	MAT	MAP	EC Processing Reference	EC Data Source	EC Site Name
ABS-UF	archboldpnot	archboldpnot	grazing	22.7	1000	Gomez-Casanovas et al., 2020	LTAR	US-IL1
ABS-UF	ufona	ufona	grazing	22.2	1007	Gomez-Casanovas et al., 2020	LTAR	US-ONA
CAF	boydnorth	cafboydnorthltar01	cropland	8.6	424	Russell et al., 2019	Ameriflux	US-CF1
CAF	cookeast	cafcookeastltar01	cropland	8.5	456	Russell et al., 2019	Ameriflux	US-CF2
CAF	cookwest	cafcookwestltar01	cropland	8.5	456	Russell et al., 2019	Ameriflux	US-CF3
CMRB	asp	goodwater	cropland	12.1	1015	Wood et al., 2019	LTAR	US-Mo1
CPER	agm	cperagm	grazing	8.2	320	NA	LTAR	US-CX2
CPER	tgm	cpertgm	grazing	8.2	320	NA	LTAR	US-CX1
GACP	arsgacp1	arsgacp1	integrated	19.0	1073	Russell et al., 2019	LTAR	NA
GACP	arsgacp2	arsgacp2	integrated	19.1	1084	Russell et al., 2019	LTAR	NA
GB	arsgreatbasinltar098	arsgreatbasinltar098	grazing	8.5	335	Flerchinger et al., 2020	LTAR	US-Rws
JORN	jerbajada	jerbajada	grazing	15.3	248	Wutzler et al. 2018	LTAR	US-Jo1
JORN	neon	NEON.D14.JORN.DP1.00033	grazing	15.4	235	Metzger et al., 2019	NEON	NEON.D14.JORN.DP4.00200.001
KBS	T3	kelloggcorn	cropland	9.5	867	Abraha et al., 2014	LTAR	US-KM1
KONA	KONA	NEON.D06.KONA.DP1.00033	cropland	12.3	843	Metzger et al., 2019	NEON	NEON.D06.KONA.DP4.00200.001
LCB	op3	arsope3ltar	cropland	12.8	1045	NA	LTAR	US-OPE
NP	mandanh	mandanh5	cropland	5.8	439	Saliendra et al., 2018	LTAR	US-NP1
NP	mandani	mandani2	cropland	5.6	431	Saliendra et al., 2018	LTAR	US-NP2
PRHPA	mead1	mead1	cropland	10.2	727	Suyker et al., 2005	LTAR	US-Ne1
PRHPA	mead2	mead2	cropland	10.2	727	Suyker et al., 2005	LTAR	US-Ne2
PRHPA	mead3	mead3	cropland	10.2	727	Suyker et al., 2005	LTAR	US-Ne3
PRHPA	meadpasture	meadpasture	grazing	10.2	726	Suyker et al., 2005	LTAR	NA
SEG	grasslands	sevilletagrass	grazing	13.9	200	Anderson-Teixeira et al., 2011	Ameriflux	US-Seg
SEG	shrublands	sevilletashrub	grazing	14.0	201	Anderson-Teixeira et al., 2011	Ameriflux	US-Ses
TG	tworfpr	tworfpr	integrated	19.0	863	NA	LTAR	US-Tx2
UCB	hawbeckereddy	hawbeckereddy	integrated	9.8	922	Skinner, 2008	LTAR	US-HWB
UMRB	morrisnorth	arsmorris1	cropland	5.8	565	Saliendra et al., 2018	LTAR	NA
UMRB	morrissouth	arsmorris2	cropland	5.8	565	Saliendra et al., 2018	LTAR	NA
UMRB	rosemountcons	rosemountcons	cropland	7.3	802	Griffis et. al., 2005	Ameriflux	US-Ro4
UMRB	rosemountconv	rosemountconv	cropland	7.3	802	Griffis et. al., 2005	Ameriflux	US-Ro5
UMRB	rosemountnprs	rosemountnprs	cropland	7.3	765	Griffis et. al., 2005	Ameriflux	US-Ro6
WGEW	Kendall Grassland	kendall	grazing	17.1	278	Scott et al., 2015	Ameriflux	US-Wkg
WGEW	Lucky Hills Shrubland	luckyhills	grazing	17.5	263	Scott et al., 2015	Ameriflux	US-Whs
NEON-Wood	USxWD	NEON.D09.WOOD.DP1.00033	grazing	4.5	430	Metzger et al., 2019	NEON	NEON.D09.WOOD.DP4.00200.001